

Variance reduction for forces and pressure in variational Monte Carlo

David Linteau,^{1,2} Saverio Moroni,³ Giuseppe Carleo,^{1,2} and Markus Holzmann⁴

¹⁾*Institute of Physics, École Polytechnique Fédérale de Lausanne (EPFL), CH-1015 Lausanne, Switzerland*

²⁾*Center for Quantum Science and Engineering, École Polytechnique Fédérale de Lausanne (EPFL), CH-1015 Lausanne, Switzerland*

³⁾*CNR-IOM DEMOCRITOS, Istituto Officina dei Materiali and SISSA Scuola Internazionale Superiore di Studi Avanzati, Via Bonomea 265, I-34136 Trieste, Italy*

⁴⁾*Univ. Grenoble Alpes, CNRS, LPMMC, 38000 Grenoble, France*

We present simple and practical strategies to reduce the variance of Monte Carlo estimators. Our focus is on variational Monte Carlo calculations of atomic forces and pressure in electronic systems, although we show that the underlying ideas apply more broadly to other observables, like pair-correlation and angular-distribution functions, and other methods, including molecular dynamics. For Pulay-type contributions, we show that a minor modification based on the Metropolis acceptance ratio softens the power-law divergence of the variance to a logarithmic one, and that inexpensive regularizations can further suppress outliers at the price of a controlled small bias. For Hellmann-Feynman forces, we derive compact variance-reduced estimators for periodic systems that are straightforward to implement in standard Monte Carlo codes. The approach is illustrated for high-pressure metallic hydrogen with more than a hundred atoms described by neural quantum states, including an application to molecular dynamics driven by the improved forces.

I. INTRODUCTION

Accurate evaluation of atomic forces and the stress tensor is central to first-principles studies of quantum many-body systems. Forces determine equilibrium geometries, vibrational properties, and the atomic-scale dynamics in molecules and condensed matter systems^{1,2}. Likewise, the stress (or pressure) underpins equations of state, elastic responses, and structural phase transitions^{3,4}. Among first-principles approaches, Variational Monte Carlo (VMC) offers a simple yet systematically improvable framework for describing strongly correlated electrons and quantum nuclei, especially with neural quantum state (NQS) wave functions that now routinely reach the accuracy of previous diffusion Monte Carlo (DMC) calculations^{5–14}.

Within VMC, it is possible to obtain force fields $\mathbf{F}(\mathbf{R}) = -\nabla_{\mathbf{R}}E(\mathbf{R})$ which are consistent with the variational Born-Oppenheimer energy surface $E(\mathbf{R}) = \langle \Psi(\mathbf{R}) | H_{\mathbf{R}} | \Psi(\mathbf{R}) \rangle / \langle \Psi(\mathbf{R}) | \Psi(\mathbf{R}) \rangle$. Here, $|\Psi(\mathbf{R})\rangle$ represents the variational approximation to the ground state of the electronic Hamiltonian $H_{\mathbf{R}}$, both of which depend parametrically on the nuclear positions \mathbf{R} . The total derivative with respect to nuclear position can then readily be calculated, leading to consistent conservative force fields (up to unavoidable stochastic noise). Foundation model wave functions^{15–17} are particularly attractive because they deliver well-defined and consistent forces across many nuclear configurations at far lower cost than re-optimizing from scratch at each geometry. While it is possible to obtain consistent forces within DMC^{18,19}, it involves averaging (and extrapolating) over the imaginary time history, which is avoided in a pure VMC framework.

However, directly differentiating the VMC energy expectation value typically leads to large statistical fluctuations.

These arise both from the singular behavior of estimators at electron-nucleus coalescence points, and from the electronic wave function approaching the nodes.

A variety of approaches have already been proposed to address these challenges²⁰. Early work focused on coordinate transformations and correlated sampling, notably the space-warp coordinate transformation^{21–23}. A second line of work constructed renormalized estimators obeying the zero-variance/zero-bias principle^{24–27}. Finally, others methods proposed isolating and fitting the short-range singular contribution, possibly combined with antithetic sampling²⁸.

These methods have mostly focused on estimators for the Hellmann-Feynman force $-\nabla_{\mathbf{R}}H_{\mathbf{R}}$, where they significantly reduce the variance and improve the reliability of the results. Methods to cure the variance problems occurring in the Pulay (or wave function) term due to the parametric dependence of the approximate ground state wave function have been addressed differently. They either modify the weight of the Monte Carlo sampling through a guiding wave function^{29–31}, introduce a regularization leading to a small systematic bias³², or introduce a warp regularization that requires the associated Jacobian and derivatives of the local energy¹⁸. We also note that other lines of work address heavy-tailed QMC statistics through alternative sampling and tail-aware error analysis^{33–35}.

In this work, we focus on variance issues in both the Hellmann-Feynman and Pulay contributions, and propose practical estimators for forces and pressure in periodic systems, with straightforward extensions to open boundaries. Building on earlier developments, especially by Assaraf and Caffarel^{24–26}, we derive expressions that add minimal (implementation) overhead in standard VMC codes and avoid introducing system-dependent tuning parameters or externally chosen numerical cutoffs

for improved Hellmann-Feynman estimators.

For the Pulay terms, we revisit an acceptance trick proposed nearly half a century ago³⁶ and show that it can attenuate the variance spikes induced by the nodal surface, improving the variance scaling from polynomial to logarithmic with the distance to the nodes. As a result, the residual bias introduced by subsequent regularization schemes^{18,32} can generally be made negligible compared with the associated statistical uncertainty. More broadly, this acceptance trick provides a systematic and essentially cost-free route to reducing the variance of a wide class of estimators.

Although we focus on forces and pressure in the presentation and the numerical results, the methods described here apply more broadly to any parameter-dependent expectation values. This includes, in particular, energy optimization, time-dependent variational Monte Carlo^{37–43}, and the infinite-variance problems that arise generically in fermionic quantum Monte Carlo calculations^{44,45}. We also discuss a related strategy that extends beyond derivative-based estimators to density-like observables sampled in Monte Carlo or molecular dynamics.

In the following, we first derive the general decomposition of energy derivatives into Hellmann-Feynman and Pulay contributions, and specialize the resulting expressions to atomic forces and pressure. We then introduce several practical variance-reduction strategies, including covariance forms for Pulay estimators, an acceptance-based treatment of nodal divergences, and integrations-by-parts constructions for Hellmann-Feynman forces in both open and periodic systems. Finally, we illustrate these ideas on high-pressure hydrogen described by a NQS, including applications to pressure, forces, molecular dynamics and pair correlations. Most derivations and additional details are provided in the appendices.

II. VARIATIONAL MONTE CARLO: DEFAULT ESTIMATORS

Consider a Hamiltonian $H(p)$ depending on a set of parameters p , and an explicit (not necessarily normalized) trial state $|\Psi(p)\rangle$ defined consistently with the chosen boundary conditions for all p of interest. Within VMC, we sample the electronic configurations $\mathbf{r} = (\mathbf{r}_1, \dots, \mathbf{r}_N)$ from the probability density $\pi(\mathbf{r}|p) \equiv |\Psi(\mathbf{r}|p)|^2 / (\int d\mathbf{r} |\Psi(\mathbf{r}|p)|^2)$, where $\Psi(\mathbf{r}|p) = \langle \mathbf{r} | \Psi(p) \rangle$ is the parameter dependent electronic wave function. For any observable A , the standard VMC estimator is the corresponding local quantity $A_L = \langle \mathbf{r} | A | \Psi(p) \rangle / \Psi(\mathbf{r}|p)$. The variational energy is obtained by averaging local energy instances evaluated at configurations distributed according to the density $\pi(\mathbf{r}|p)$, that is,

$$E(p) = \langle H_p \rangle = \mathbb{E}_{\mathbf{r} \sim \pi(\mathbf{r}|p)} [E_L(\mathbf{r}|p)], \quad (1)$$

where the local energy is defined as follows

$$E_L(\mathbf{r}|p) = \frac{\langle \mathbf{r} | H(p) | \Psi(p) \rangle}{\Psi(\mathbf{r}|p)}. \quad (2)$$

We will often abbreviate configuration-space averages over $\pi(\mathbf{r}|p)$ using the bra-ket (expectation value) notation

$$\langle A \rangle \equiv \mathbb{E}_{\mathbf{r} \sim \pi(\mathbf{r}|p)} [A_L(\mathbf{r}|p)], \quad (3)$$

and drop the explicit dependence on p .

In the case of nuclear forces and pressure, discussed below, we will consider the electronic Hamiltonian at fixed nuclear positions \mathbf{R} ,

$$H_{\mathbf{R}} = K_e(\mathbf{r}) + V_{ee}(\mathbf{r}) + V_{en}(\mathbf{r}, \mathbf{R}) + V_{nn}(\mathbf{R}), \quad (4)$$

where $K_e(\mathbf{r}) = -\hbar^2/(2m) \sum_i \nabla_{\mathbf{r}_i}^2$ is the electronic kinetic energy operator. Here V_{ee} , V_{en} , and V_{nn} are the electron-electron, electron-ion, and ion-ion Coulomb interactions, respectively, for electrons of charge $-e$ and nuclei of charge $Z_I e$ (with I being the nuclear index). Under the Born-Oppenheimer approximation, the nuclear degrees of freedom enter the Hamiltonian $H_{\mathbf{R}}$ only parametrically through their coordinates $\mathbf{R} = (\mathbf{R}_1, \dots, \mathbf{R}_N)$.

A. General parameter optimization

Given $H(p)$ and $|\Psi(p)\rangle$, as defined in the previous section, we introduce the corresponding variational energy surface

$$E(p) = \frac{\langle \Psi(p) | H(p) | \Psi(p) \rangle}{\langle \Psi(p) | \Psi(p) \rangle}, \quad (5)$$

which, for each fixed p , is an upper bound to the exact ground state energy of $H(p)$.

We are not only interested in the energy $E(p)$ for given values of p , but also in its derivative with respect to p . Assuming a sufficiently smooth parameter dependence of the Hamiltonian and the trial wave function, we have

$$\frac{\partial E}{\partial p} = \underbrace{\frac{\langle \Psi | \partial_p H | \Psi \rangle}{\langle \Psi | \Psi \rangle}}_{\text{Hellmann-Feynman (operator) term}} + 2\text{Re} \underbrace{\frac{\langle \Psi | H - E | \partial_p \Psi \rangle}{\langle \Psi | \Psi \rangle}}_{\text{Pulay (wave function) term}}. \quad (6)$$

In the case where $|\Psi(p)\rangle$ is proportional to an exact eigenstate, so that $H(p)|\Psi(p)\rangle = E(p)|\Psi(p)\rangle$, the Pulay term clearly vanishes. More generally, it is sufficient that the energy functional $E(p, |\phi\rangle) = \langle \phi | H_p | \phi \rangle / \langle \phi | \phi \rangle$ be stationary, at fixed p , with respect to variations along the direction $|\partial_p \Psi\rangle$, i.e. within the subspace $|\phi\rangle = |\Psi(p)\rangle + \lambda |\partial_p \Psi\rangle$. Although this stationarity condition may be satisfied at isolated parameter values p_0 , enforcing it along an entire continuous path in parameter space is much more restrictive. As a result, both the Hellmann-Feynman and Pulay contributions should generally be retained to obtain the correct energy derivative.

For pure energy-minimization problems, the Hamiltonian is parameter independent, so the Hellmann-Feynman contribution vanishes and only the Pulay term

remains,

$$\frac{\partial E(p)}{\partial p} = 2\text{Re} \left\langle [E_L(\mathbf{r}) - E(p)] \partial_p \log \Psi^*(\mathbf{r}|p) \right\rangle. \quad (7)$$

Since this term can be written as a covariance (a form that we will leverage in Section III A),

$$\frac{\partial E(p)}{\partial p} = 2\text{Re} \text{Cov}(E_L, \partial_p \log \Psi^*), \quad (8)$$

its magnitude is bounded by the product of the corresponding variances via the Cauchy-Schwarz inequality,

$$\left| \frac{\partial E(p)}{\partial p} \right| \leq 2\sqrt{\text{Var}(E_L)\text{Var}(\partial_p \log \Psi^*)}. \quad (9)$$

This makes explicit how the zero-variance principle provides an analytical guarantee: as the trial wave function approaches an exact eigenstate, $\text{Var}(E_L) \rightarrow 0$, so the Pulay contribution is automatically suppressed, provided $\text{Var}(\partial_p \log \Psi^*)$ remains finite.

However, higher moments of the Pulay estimator in general do not exist. Indeed, the Pulay estimator behaves as $|\Psi|^{-2}$ approaching the nodes,

$$\partial_p E \sim E_L \partial_p \log \Psi^* \sim \left(\frac{\nabla_{\mathbf{r}}^2 \Psi}{\Psi} \right) \left(\frac{\partial_p \Psi^*}{\Psi^*} \right) \sim |\Psi|^{-2}, \quad (10)$$

given that the Laplacian of the local energy, $\nabla_{\mathbf{r}}^2 \Psi(\mathbf{r}|p)$, as well as $\partial_p \Psi^*(\mathbf{r}|p)$ generally do not vanish at the nodes of $\Psi(\mathbf{r}|p)$. The mean remains finite because the sampling weight $\pi \propto |\Psi|^2$ suppresses this behavior at the nodes. On the other hand, the second moment of the Pulay estimator, involving $|\Psi|^{-4}$, will cause the variance to diverge. This divergence will generically show up in all Pulay terms occurring in parameter derivatives of general observables involving fermionic wave functions. We will show below how an acceptance trick helps to control the derivative in practice.

So far, we have focused on pure energy minimization, for which the Hamiltonian is parameter independent and only the Pulay term survives. This changes for observables such as atomic forces and pressure, which are obtained by differentiating the energy with respect to parameters that enter the Hamiltonian explicitly, so that both Hellmann-Feynman and Pulay terms contribute. We now turn first to forces and then to pressure.

B. Nuclear forces

Within the Born-Oppenheimer approximation, recall that the nuclear coordinates \mathbf{R} enter the electronic Hamiltonian $H_{\mathbf{R}}$, defined in Eq. (4), only as parameters. The Hellmann-Feynman force on nucleus I then reads

$$\mathbf{F}_I^{\text{HF}} = -\langle \nabla_{\mathbf{R}_I} H_{\mathbf{R}} \rangle. \quad (11)$$

Stochastic fluctuations will only come from the electron-nucleus term

$$-\langle \nabla_{\mathbf{R}_I} V_{en} \rangle = -\sum_i \langle \nabla_{\mathbf{R}_I} v_{en}(\mathbf{R}_I - \mathbf{r}_i) \rangle \quad (12)$$

$$= \int d^3\mathbf{u} \mathbf{f}(\mathbf{u}) \rho(\mathbf{R}_I - \mathbf{u}), \quad (13)$$

where $\mathbf{f}(\mathbf{u}) = -\nabla v_{en}(\mathbf{u})$ is the electron-nucleus force kernel and $\rho(\mathbf{u}) = \langle \sum_{i=1}^N \delta(\mathbf{u} - \mathbf{r}_i) \rangle$ is the electronic density.

To keep the expressions compact, we introduce the electron-nucleus relative vector as $\mathbf{x}_{iI} \equiv \mathbf{r}_i - \mathbf{R}_I$, the associated distance $x_{iI} = |\mathbf{x}_{iI}|$, and the α -component $x_{iI,\alpha} \equiv (\mathbf{x}_{iI})_{\alpha}$. When no confusion can arise, we omit particle indices and simply write \mathbf{x} , with $x = |\mathbf{x}|$. For isolated systems (open boundary conditions), $v_{en}(x) \sim 1/x$, while for extended systems (periodic boundary conditions), v_{en} must be modified to account for the interaction with periodic images, which is typically handled using Ewald summation⁴⁶. In practice, this is achieved by splitting the interaction into short- and long-range parts,

$$v_{en}(x) = v_{en}^{sr}(x) + v_{en}^{lr}(x), \quad (14)$$

where v_{en}^{sr} retains the $1/x$ behavior at small x , while the long-range component v_{en}^{lr} is evaluated in Fourier space.

While the long-range contribution to the Hellmann-Feynman force is typically well behaved, the short-range part leads to a singular force kernel $\mathbf{f}(\mathbf{x}) \sim \mathbf{x}/x^3$ as $x \rightarrow 0$. Since the electronic density remains finite at the nucleus, $\rho(\mathbf{R}_I - \mathbf{u}) \simeq \rho(\mathbf{R}_I) \neq 0$, the integral in Eq. (13) remains finite, and \mathbf{F}_I^{HF} is therefore an unbiased estimator of the Hellmann-Feynman force. The variance, however, diverges because the second moment involves $\mathbf{f}^2(\mathbf{u}) \sim u^{-4}$, yielding

$$\int d^3\mathbf{u} \mathbf{f}^2(\mathbf{u}) \rho(\mathbf{R}_I - \mathbf{u}) \simeq 4\pi \rho(\mathbf{R}_I) \int_0^{\epsilon} u^{-2} du \rightarrow \infty, \quad (15)$$

as $\epsilon \rightarrow 0$. In this work, we will show how this divergence can be cured in simple ways.

The Pulay force has the general form given in Eq. (7), and its variance diverges, as described in Section II A, due to the fermionic nodes. In practice, however, this divergence is usually not severe for forces given that $\partial_{R_{I,\alpha}}$ acts locally (as compared to the pressure as we will discuss next), and as long as the fluctuations of $\Delta E \equiv E_L(\mathbf{r}) - E(p)$ away from 0 are not large (which is typically the case when the trial wave function is close to the ground state). This will be shown in the Results section.

C. Pressure

As a second key observable, we consider the thermodynamic pressure, $P = -\partial E / \partial \Omega$, where $\Omega = L_x L_y L_z$ is the volume of an orthorhombic simulation cell of size

$\mathbf{L} = (L_x, L_y, L_z)$. (This choice is made for clarity; the derivation generalizes straightforwardly to a non-orthorhombic cell by replacing \mathbf{L} with the cell matrix \mathbf{h} and $\Omega = \text{deth}$.) An isotropic volume change is parameterized by a scale factor s via $L_\alpha \rightarrow sL_\alpha$, for all $\alpha \in \{x, y, z\}$, so that $\Omega \rightarrow s^3\Omega$ and

$$P = -\frac{\partial E}{\partial \Omega} = -\frac{1}{3\Omega} \frac{dE(s)}{ds} \Big|_{s=1}, \quad (16)$$

where $E(s) \equiv E(\mathbf{R}(s), \mathbf{L}(s))$.

Although the box lengths can be viewed as parameters, this derivative cannot be taken naively using Eq. (6), because changing \mathbf{L} modifies the boundary conditions of the wave function ($\Psi(\mathbf{r}_i + \mathbf{L}|\mathbf{L}) = \Psi(\mathbf{r}_i|\mathbf{L})$ under periodic boundary conditions), which violates an implicit assumption behind Eq. (6). To proceed, we therefore introduce scaled coordinates $\tilde{\mathbf{r}}_i = \mathbf{r}_i\mathbf{L}^{-1}$ and $\tilde{\mathbf{R}}_I = \mathbf{R}_I\mathbf{L}^{-1}$, so that the wave function of the scaled box reads

$$\tilde{\Psi}(\tilde{\mathbf{r}}|\tilde{\mathbf{R}}, \mathbf{L}) = \Omega^{N/2}\Psi(\tilde{\mathbf{r}}\mathbf{L}|\tilde{\mathbf{R}}\mathbf{L}, \mathbf{L}), \quad (17)$$

with $\Omega^{N/2}$ being the square root of the Jacobian of the transformation $d\mathbf{r}_i = \Omega d\tilde{\mathbf{r}}_i$ (for all $1 \leq i \leq N$) needed so that $|\tilde{\Psi}|^2 d\tilde{\mathbf{r}}$ represents the same probability measure as $|\Psi|^2 d\mathbf{r}$. The associated scaled Hamiltonian is

$$\tilde{H}_{\tilde{\mathbf{R}}, \mathbf{L}} = \tilde{K}_e(\tilde{\mathbf{r}}\mathbf{L}) + V_{ee}(\tilde{\mathbf{r}}\mathbf{L}) + V_{en}(\tilde{\mathbf{r}}\mathbf{L}, \tilde{\mathbf{R}}) + V_{nn}(\tilde{\mathbf{R}}\mathbf{L}), \quad (18)$$

where $\tilde{K}_e(\tilde{\mathbf{r}}) = -\hbar^2/(2m) \sum_{i,\alpha} L_\alpha^{-2} \partial_{\tilde{r}_{i\alpha}}^2$. By construction, $\tilde{\Psi}$ satisfies the periodic boundary conditions on the unit box $[0, 1]^3$, independently of \mathbf{L} , so partial derivatives with respect to \mathbf{L} (or s) are therefore well defined. We can thus apply the general parameter-derivative formula given in Eq. (6) to \tilde{H} and $\tilde{\Psi}$, and then re-express the final results in terms of the original H and Ψ .

Defining the shorthands $\tilde{\Psi}_s \equiv \tilde{\Psi}(\cdot|\tilde{\mathbf{R}}, \mathbf{L}(s))$ and $\tilde{H}_s \equiv \tilde{H}_{\tilde{\mathbf{R}}, \mathbf{L}(s)}$, the variational energy reads

$$E(s) = \frac{\langle \tilde{\Psi}_s | \tilde{H}_s | \tilde{\Psi}_s \rangle}{\langle \tilde{\Psi}_s | \tilde{\Psi}_s \rangle}, \quad (19)$$

and its derivative decomposes into the usual Hellmann-Feynman (Virial) and wave function (Pulay) contributions,

$$\frac{dE}{ds} = \langle \partial_s \tilde{H}_s \rangle_{\tilde{\pi}} + 2\text{Re} \left\langle (\tilde{E}_L - E) \partial_s \log \tilde{\Psi}_s^* \right\rangle_{\tilde{\pi}}, \quad (20)$$

where $\tilde{\pi} \propto |\tilde{\Psi}_s|^2$ and $\tilde{E}_L = (\tilde{H}_s \tilde{\Psi}_s) / \tilde{\Psi}_s$. The pressure splits accordingly, $P = P^V + P^{wf}$. For pure Coulomb interactions, the explicit derivative of the scaled Hamiltonian, $\partial_s \tilde{H}_s$, yields the usual Virial estimator⁴

$$P^V = \frac{1}{3\Omega} (2K_e + V), \quad (21)$$

with $V = V_{ee} + V_{en} + V_{nn}$. In contrast to the nuclear forces above, the standard (unbiased) estimator for P^V already has finite variance.

Rewriting the wave function contribution in terms of the original Ψ gives

$$P^{wf} = -\frac{2}{3\Omega} \text{Re} \left\langle \Delta E(\mathbf{r}|\mathbf{R}, \mathbf{L}) \mathcal{D} \log \Psi^*(\mathbf{r}|\mathbf{R}, \mathbf{L}) \right\rangle, \quad (22)$$

where $\Delta E(\mathbf{r}|\mathbf{R}, \mathbf{L}) \equiv E_L(\mathbf{r}|\mathbf{R}, \mathbf{L}) - E(\mathbf{R}, \mathbf{L})$, and we conveniently introduced the dilation operator

$$\mathcal{D} \equiv \frac{d}{ds} \Big|_{s=1} = \mathbf{r} \cdot \nabla_{\mathbf{r}} + \mathbf{R} \cdot \nabla_{\mathbf{R}} + \mathbf{L} \cdot \nabla_{\mathbf{L}}, \quad (23)$$

which, as the name suggests, is a generator of isotropic scaling (preserving the relative geometry within the cell). Upon writing the scaled wave function explicitly along the path $\mathbf{L}(s) = s\mathbf{L}$,

$$\tilde{\Psi}(\tilde{\mathbf{r}}|\tilde{\mathbf{R}}, \mathbf{L}(s)) = \Omega(\mathbf{L}(s))^{N/2} \Psi(\tilde{\mathbf{r}}\mathbf{L}(s)|\tilde{\mathbf{R}}\mathbf{L}(s), \mathbf{L}(s)), \quad (24)$$

one finds $\Omega(\mathbf{L}(s)) = s^3\Omega(\mathbf{L})$ and therefore

$$\mathcal{D} \log \tilde{\Psi}^* = \mathcal{D} \log \Psi^* + \frac{3N}{2}. \quad (25)$$

We note that this construction can be extended beyond the pressure to the off-diagonal elements of the stress tensor.

III. VARIANCE REDUCTION METHODS

Above, we have seen that the standard force estimator and Pulay contributions (for forces and pressure) have divergent second moments, so that the error of a Monte Carlo simulation with finite statistics cannot be estimated by standard methods based on the central limit theorem⁴⁷. In the following, we present simple and practical methods for addressing these variance problems, still focusing on force and pressure calculations. For detailed derivations and more sophisticated improvements, we refer to the appendices.

A. Covariance

Consider the standard Pulay estimator given in Eq. (7), which, as hinted previously in Section II A, can be recast in the equivalent covariance form

$$\frac{\partial E}{\partial p} = 2\text{Re} \left\langle \Delta E [\partial_p \log \Psi^* - \langle \partial_p \log \Psi^* \rangle] \right\rangle. \quad (26)$$

Crucially, the subtraction of $\langle \partial_p \log \Psi^* \rangle$ provides a simple but powerful variance-reduction trick, as it leaves the mean unchanged (since $\langle \Delta E \rangle = 0$) while typically reducing fluctuations substantially^{48,49}.

In the case of pressure, for example, where ∂_p is replaced by the dilation derivative \mathcal{D} introduced in Eq. (23), this covariance formulation is especially valuable because it cancels the constant offset $3N/2 \sim \mathcal{O}(N)$ appearing in Eq. (25), preventing this extensive constant from inflating the variance despite not contributing to the mean.

B. Acceptance trick

The Metropolis acceptance-ratio trick discussed in this section was already mentioned in the pioneering work of Ceperley, Chester and Kalos³⁶. To our knowledge, despite being introduced nearly half a century ago, this variance-reduction idea has not been revisited or analyzed in detail in the subsequent QMC literature. We therefore take the opportunity to revisit it here, formalize its near-node behavior by showing how it reduces the variance divergence from power-law to logarithmic (with respect to the distance to the nodal surface), and extend it to a regularized form with controlled bias.

The method exploits additional information available in the Metropolis-Hastings accept/reject step of the Markov chain. Consider a proposed move from an initial configuration \mathbf{r}_i to a proposed configuration \mathbf{r}_f . The move is then accepted with probability

$$a \equiv a(\mathbf{r}_i \rightarrow \mathbf{r}_f) = \min \left(1, \frac{\pi(\mathbf{r}_f)p(\mathbf{r}_i|\mathbf{r}_f)}{\pi(\mathbf{r}_i)p(\mathbf{r}_f|\mathbf{r}_i)} \right), \quad (27)$$

where π is the target distribution, taken to be the Born distribution $\pi(\mathbf{r}) = |\Psi(\mathbf{r})|^2$ in VMC, and $p(\mathbf{x}|\mathbf{y})$ is the proposal distribution to sample \mathbf{x} given \mathbf{y} . Instead of evaluating an observable $O(\mathbf{r})$ only at the configuration obtained after the accept/reject step, one can use the conditional estimator³⁶

$$\tilde{O}(\mathbf{r}_i, \mathbf{r}_f) = aO(\mathbf{r}_f) + (1-a)O(\mathbf{r}_i), \quad (28)$$

which is defined independently of whether the proposal is ultimately accepted. In other words, the acceptance probability is used to form a weighted average of the estimator evaluated at the initial and proposed configurations.

This construction is a simple instance of the Rao-Blackwell theorem^{20,50–52}: rather than using the post-acceptance value $O(\mathbf{r}_{i+1})$, one replaces it by its conditional expectation given $(\mathbf{r}_i, \mathbf{r}_f)$. Once the Markov chain has thermalized, this estimator remains unbiased,

$$\begin{aligned} \mathbb{E}[\tilde{O}(\mathbf{r}_i, \mathbf{r}_f)] &= \mathbb{E}_{\mathbf{r}_i \sim \pi} \mathbb{E}_{\mathbf{r}_f \sim p(\mathbf{r}_f|\mathbf{r}_i)} \mathbb{E}_A [O(\mathbf{r}_{i+1}|\mathbf{r}_i, \mathbf{r}_f)] \\ &= \mathbb{E}[O(\mathbf{r}_{i+1})] = \langle O \rangle, \end{aligned} \quad (29)$$

where $A \in \{0, 1\}$ is the Metropolis-Hastings acceptance indicator with $A \sim \text{Bernoulli}(a(\mathbf{r}_i \rightarrow \mathbf{r}_f))$, and $\mathbf{r}_{i+1} = A\mathbf{r}_f + (1-A)\mathbf{r}_i$. Moreover, the Rao-Blackwell theorem guarantees that this replacement can only reduce the variance, or leave it unchanged, that is,

$$\text{Var}(\tilde{O}(\mathbf{r}_i, \mathbf{r}_f)) \leq \text{Var}(O(\mathbf{r}_{i+1})). \quad (30)$$

The acceptance trick can therefore be applied on top of essentially any estimator $O(\mathbf{r})$ as a cheap post-processing improvement to reduce numerical instabilities. In the following, we focus on its impact on Pulay terms. Our discussion concentrates on the variance problems induced by nodal singularities, which are the most common source of

large fluctuations. We will always assume that $\partial_p \log \Psi$ has finite variance, and exclude too strong explicit singularities (which would require separate considerations, analogous to those used for Hellmann-Feynman estimators discussed below). Under these assumptions, we show that the acceptance trick can systematically mitigate the variance problems in Pulay terms.

C. Regularization of Pulay terms

We now build on top of the previous ‘‘Acceptance trick’’ Section, and focus on the general Pulay estimator given in Eq. (7), of the form $O(\mathbf{r}) \sim (E_L(\mathbf{r}) - E)\partial_p \log \Psi^*(\mathbf{r})$, and analyze its behavior close to the nodes, where $\Psi(\mathbf{r}) \equiv \Psi(\mathbf{r}|p) = 0$ (dropping the dependence on p for this discussion). In the vicinity of a node, we introduce local coordinates $\mathbf{r} = (\xi, \mathbf{r}_\parallel)$, where ξ is the normal coordinate, i.e. the signed distance to the nodal surface, and \mathbf{r}_\parallel denotes the tangential coordinates. We can then expand the wave function along the normal coordinate ξ as $\Psi(\xi, \mathbf{r}_\parallel) = \partial_\xi \Psi(\xi, \mathbf{r}_\parallel)|_{\xi=0} \xi + \mathcal{O}(\xi^2)$, so that the wave function vanishes linearly to leading order,

$$\Psi(\xi, \mathbf{r}_\parallel) \approx \Phi(\mathbf{r}_\parallel)\xi, \quad (31)$$

with $\Phi(\mathbf{r}_\parallel) \equiv \partial_\xi \Psi(\xi, \mathbf{r}_\parallel)|_{\xi=0} \neq 0$, so that $|\Psi|^2 \sim \xi^2$. Generically, both $H\Psi$ and $\partial_p \Psi$ approach non-zero constants as $\xi \rightarrow 0$. It follows that $E_L = H\Psi/\Psi \sim \xi^{-1}$ and $\partial_p \log \Psi^* = \partial_p \Psi^*/\Psi^* \sim \xi^{-1}$, which in turn implies that the Pulay estimator behaves as $(E_L - E)\partial_p \log \Psi^* \sim \xi^{-2}$. Because the sampling weight vanishes as $|\Psi|^2 \sim \xi^2$, the mean remains finite. The variance, however, involves the second moment ξ^{-4} of the estimator, which leads to a divergent integral $\int \xi^2 \xi^{-4} d\xi$ and the default power-law divergence scaling of $\mathcal{O}(1/\xi_c)$, where ξ_c is a short-distance length scale introduced only to display the divergence of unregularized estimators.

A simple regularization scheme is to exclude a small region of width ϵ around the nodes by multiplying the integrand by a Heaviside step function $\theta_\epsilon(\xi) \equiv \theta(|\xi| - \epsilon)$, that vanishes for $|\xi| < \epsilon$. This makes the variance finite, of order $\mathcal{O}(1/\epsilon)$, but introduces a bias, of order $\mathcal{O}(\epsilon)$, because the discarded region obviously contributes to the mean. A clever choice of a smoother regularizing function³² can actually reduce the bias to order ϵ^3 .

Let us instead use the acceptance trick together with a simple step-function regularization. Rather than applying the cutoff symmetrically, we apply it only to the current configuration \mathbf{r}_i inside the conditional estimator, that is,

$$\tilde{O}_\epsilon(\mathbf{r}_i, \mathbf{r}_f) = \theta_\epsilon(\xi_i) \left[aO(\mathbf{r}_f) + (1-a)O(\mathbf{r}_i) \right], \quad (32)$$

where ξ_i is the orthogonal distance to the nodal surface of \mathbf{r}_i . Inserting the near-node behavior of the wave function ($\Psi \sim \xi$) into this expression shows that the bias scales as $\mathcal{O}(\epsilon^2)$, while the variance grows only logarithmically,

$\text{Var}(\tilde{O}_\epsilon) \sim \log(1/\epsilon)$. This logarithmic behavior is a direct consequence of the acceptance trick, and should be contrasted with the default estimator, whose variance scales as $\mathcal{O}(1/\epsilon)$.

Due to the very mild logarithmic divergence of the variance, one can choose ϵ small enough that the $\mathcal{O}(\epsilon^2)$ bias is negligible compared with statistical uncertainties. Alternatively, one may eliminate the residual bias systematically by performing an explicit $\epsilon \rightarrow 0$ extrapolation, as proposed by Pathak and Wagner³².

In Section A, we analyze these asymptotic scalings in detail for the three regularized acceptance-based estimators introduced there: the ‘‘one-point’’ hard cutoff $\tilde{O}_\epsilon^{(1)}$, corresponding to Eq. (32), the ‘‘two-point’’ hard cutoff $\tilde{O}_\epsilon^{(2)}$ (generalizing the cutoff $\theta_\epsilon(\xi_i)$ used in Eq. (32) to also include ξ_f), and the smooth-cutoff estimator \hat{O}_ϵ . In particular, we show that the two hard-cutoff forms retain the favorable logarithmic variance while introducing a $\mathcal{O}(\epsilon^2)$ bias, and that this bias can be systematically improved by replacing such ‘‘hard-cutoffs’’ with a smooth polynomial regularization function χ . If one then imposes the endpoint and smoothness conditions $\chi(0) = 0, \chi'(0) = 0, \chi(1) = 1$ and $\chi'(1) = 0$, a polynomial cutoff of degree $m+3$ is sufficient to cancel the first m bias moments and as a result obtain a residual bias of order ϵ^{m+2} for $m \geq 1$.

D. Integration by parts (for Hellmann-Feynman forces)

In contrast to the Pulay force, the standard estimator of the Hellman-Feynman (HF) force does not satisfy a zero-variance principle, meaning that the operator still fluctuates even when the wave function sampled coincides with an exact energy eigenstate. Several variance-reduction strategies have been proposed^{22,25,26,28}. In this section, we present a simple two-step approach applicable both to isolated (OBC) and extended (PBC) systems that relies on integrating by parts (IBP). The first step partially removes the coalescence singularity to leading order, while the second cancels it exactly by exploiting a ‘‘gradient-to-Laplacian’’ identity.

This key identity, rapidly derived in Section B, states that for any functions $v(x)$ and $f(x) = xv(x)$, provided $x \neq 0$,

$$2\partial_{x_\alpha} v(x) = \nabla_{\mathbf{x}}^2 [x_\alpha v(x)] - \frac{x_\alpha}{x} f''(x), \quad (33)$$

where $\partial_{x_\alpha} \equiv \partial/\partial x_\alpha$ and $\nabla_{\mathbf{x}}^2 = \nabla_{\mathbf{x}} \cdot \nabla_{\mathbf{x}}$ ($\mathbf{x} \in \mathbb{R}^3$, $x = |\mathbf{x}|$). Note here that \mathbf{x} still corresponds to the electron-nucleus relative vector $\mathbf{x}_{iI} = \mathbf{r}_i - \mathbf{R}_I$ (omitting the particle indices for ease of notation), and $\nabla_{\mathbf{x}} = \nabla_{\mathbf{r}} = (\nabla_{\mathbf{r}_1}, \dots, \nabla_{\mathbf{r}_N})$ is the configuration-space gradient. We will use $\nabla_i \equiv \nabla_{\mathbf{r}_i}$.

1. First IBP step: moving the gradient to the density

The variance problem originates from the short-range divergence of the electron-nucleus interaction v_{en} . To isolate the singular contribution, we split the interaction in a short and a long-range part (as in Eq. (14)), that is, $v_{en} = v_{en}^{sr} + v_{en}^{lr}$, where $v_{en}^{sr}(x) \sim 1/x$ as $x \rightarrow 0$. We note that this decomposition is not restricted to periodic systems, as one may set $v_{en}^{sr} = v_{en}$ and $v_{en}^{lr} = 0$ for open systems. In either case, the short-range Hellmann-Force on nucleus I can be written as

$$\mathbf{F}_{I,sr}^{\text{HF}} = - \int d^3\mathbf{u} \nabla_{\mathbf{R}_I} v_{en}^{sr}(\mathbf{R}_I - \mathbf{u}) \rho(\mathbf{u}) \quad (34)$$

$$= - \int d^3\mathbf{u} v_{en}^{sr}(\mathbf{u} - \mathbf{R}_I) \nabla_{\mathbf{u}} \rho(\mathbf{u}), \quad (35)$$

where we used $-\nabla_{\mathbf{R}_I} v_{en}^{sr}(\mathbf{R}_I - \mathbf{u}) = \nabla_{\mathbf{u}} v_{en}^{sr}(\mathbf{R}_I - \mathbf{u})$ and then integrated by parts; the boundary term vanishes both for open and periodic systems. Using $\rho(\mathbf{u}) = \langle \sum_{i=1}^N \delta(\mathbf{u} - \mathbf{r}_i) \rangle$, its gradient can be written as

$$\nabla_{\mathbf{u}} \rho(\mathbf{u}) = 2 \sum_i \left\langle \delta(\mathbf{u} - \mathbf{r}_i) \nabla_{\mathbf{r}_i} \log |\Psi| \right\rangle, \quad (36)$$

where we again integrated by parts. Inserting this identity into Eq. (35) gives the first IBP-based estimator

$$\mathbf{F}_{I,sr}^{\text{IBP1}}(\mathbf{r}) = -2 \sum_i v_{en}^{sr}(\mathbf{r}_i - \mathbf{R}_I) \nabla_{\mathbf{r}_i} \log |\Psi|, \quad (37)$$

with $\mathbf{F}_{I,sr}^{\text{HF}} = \langle \mathbf{F}_{I,sr}^{\text{IBP1}}(\mathbf{r}) \rangle$. Thanks to the electron-nucleus cusp condition $\Psi(\mathbf{x}) = \Psi(0)[1 - Z_I x + \dots]$, for $x \rightarrow 0$, the gradient behaves as $\nabla_i \log |\Psi| = \nabla_i \Psi / \Psi = (\partial_x \Psi / \Psi) \nabla_i x \sim -Z_I \mathbf{x} / x$. The IBP1 estimator therefore only scales as

$$\mathbf{F}_{I,sr}^{\text{IBP1}}(\mathbf{r}) \sim v_{en}^{sr}(x) \nabla_i \log |\Psi| \sim \frac{\mathbf{x}}{x^2} \sim \mathcal{O}\left(\frac{1}{x}\right), \quad (38)$$

compared to the default estimator scaling of $\mathbf{x}/x^3 = \hat{\mathbf{x}}/x^2 = \mathcal{O}(1/x^2)$, near coalescence points $x = |\mathbf{r}_i - \mathbf{R}_I| \rightarrow 0$. This estimator thus provides a straightforward way to partially cure the variance problem.

2. Second IBP step: gradient-to-Laplacian identity

To further reduce the fluctuations, one can trade the singular derivative of v_{en}^{sr} for a Laplacian acting on a less singular quantity, using the identity given in Eq. (33). The derivation is identical for open and periodic systems; only the choice of v_{en}^{sr} differs. For example, under OBC, $v_{en}^{sr}(x) \sim 1/x$, while under PBC, a typical choice is $v_{en}^{sr}(\mathbf{x}) = \sum_{\mathbf{T}} \text{erfc}(\kappa|\mathbf{x} + \mathbf{T}|)/|\mathbf{x} + \mathbf{T}|$, corresponding to the Ewald short-range kernel, where $\{\mathbf{T}\}$ is the set of lattice translation vectors and $\kappa > 0$ is the (fixed) Ewald screening parameter. In the following, we keep the notation shortcut $v_{en}^{sr}(x_{iI})$, with the understanding that, in

the periodic case, this denotes the periodized kernel evaluated at the relative vector $\mathbf{x}_{iI} = \mathbf{r}_i - \mathbf{R}_I$, including the implicit sum over translation vectors.

We start from the expression of the α -component of the short-range HF force on nucleus I ,

$$F_{I, sr, \alpha}^{\text{HF}} = \sum_i \int d\mathbf{r} |\Psi|^2 \partial_{x_{iI, \alpha}} v_{en}^{sr}(x_{iI}), \quad (39)$$

where we used that $-\partial_{R_{I\alpha}} = \partial_{r_{i\alpha}} = \partial_{x_{iI, \alpha}}$. We can directly recover the IBP1 estimator given in Eq. (37) by moving the partial derivative $\partial_{x_{iI, \alpha}}$ to the weight $|\Psi|^2$ using a single integration by parts. Instead, applying the gradient-to-Laplacian identity given in Eq. (33), with $v \equiv v_{en}^{sr}$ and $f(x) = xv_{en}^{sr}(x)$, we obtain

$$F_{I, \alpha, sr}^{\text{HF}} = \sum_i \left\langle \frac{\nabla_i^2 [x_{iI, \alpha} v_{en}^{sr}(x_{iI})]}{2} - \frac{x_{iI, \alpha}}{2x_{iI}} f''(x_{iI}) \right\rangle. \quad (40)$$

Integrating by parts the Laplacian term (still with vanishing boundary term), we get the following improved estimator, that we label ‘‘IBP2’’,

$$F_{I\alpha}^{\text{IBP2}}(\mathbf{r}) = - \sum_j \nabla_j Q_{I\alpha} \cdot \nabla_j \log |\Psi| - R_{I\alpha}, \quad (41)$$

$$Q_{I\alpha}(\mathbf{r}) = \sum_i \frac{x_{iI, \alpha}}{x_{iI}} f(x_{iI}), \quad (42)$$

$$R_{I\alpha}(\mathbf{r}) = \frac{1}{2} \sum_i \frac{x_{iI, \alpha}}{x_{iI}} f''(x_{iI}), \quad (43)$$

so that $\mathbf{F}_{I, sr}^{\text{HF}} = \langle \mathbf{F}_{I, sr}^{\text{IBP2}}(\mathbf{r}) \rangle$, and the \mathbf{Q} -function defined is analogous to the one introduced by Assaraf and Caffarel²⁶. Since $\nabla_j \log |\Psi| \sim \hat{\mathbf{x}}$ (as demonstrated above Eq. (38)), the only potentially singular piece arising from the first term of $\nabla_j [(x_{iI, \alpha}/x_{iI})f(x_{iI})] = f(x_{iI})\nabla_j (x_{iI, \alpha}/x_{iI}) + (x_{iI, \alpha}/x_{iI})f'(x_{iI})\nabla_j x_{iI}$ drops out because it is orthogonal to the radial direction, that is, $f(x_{iI})\nabla_j (x_{iI, \alpha}/x_{iI}) \cdot \hat{\mathbf{x}} = 0$, and $f(0)$ is finite. As a result, unlike the IBP1 estimator reported in Eq. (37), the IBP2 estimator remains finite at coalescence points.

Note that in the case of OBC, $v_{en}^{sr}(x) \sim 1/x$ and $f(x) \sim 1$ implies that $f''(x) = 0$, so $R_{I\alpha} = 0$, and Eq. (41) reduces to the Assaraf-Caffarel improved form²⁶ (derived in Section C1).

E. Further improvements

Assaraf and Caffarel²⁴ introduced a general strategy to define renormalized VMC estimators by replacing the bare observable O with a modified observable O' that has the same expectation value over the Born distribution $\pi \propto |\Psi|^2$, but typically a substantially reduced variance. Although they did not phrase their construction in terms of control variates, it can be viewed as a special case of a broader class of so-called Stein control variates, as we show in Section C1. This broader Stein operator

perspective originates from Stein’s method for distributional approximation⁵³.

A key development in this field was the generator interpretation due to Barbour^{54,55}, which observes that if \mathcal{G} is the infinitesimal generator of an ergodic Markov process with stationary distribution π , then $\langle \mathcal{G}[f] \rangle_\pi = 0$ under mild regularity and boundary conditions, for some smooth test function f . Choosing the overdamped Langevin diffusion as such a process leads to the standard Langevin Stein operator^{56,57},

$$\mathcal{L}_\pi[\mathbf{A}](\mathbf{r}) = \nabla \cdot \mathbf{A}(\mathbf{r}) + \mathbf{A}(\mathbf{r}) \cdot \nabla \log \pi(\mathbf{r}), \quad (44)$$

which satisfies $\langle \mathcal{L}_\pi[\mathbf{A}] \rangle_\pi = 0$ under mild boundary conditions and for any sufficiently regular vector field $\mathbf{A}(\mathbf{r})$; here $\nabla \equiv \nabla_{\mathbf{r}}$ is the configuration-space gradient. This identity (and related) underpins Stein-based control variates and control functional methods for variance reduction^{58,59}. For our purposes, one can define $O' \equiv O + \mathcal{L}_\pi[\mathbf{A}]$ and choose \mathbf{A} so that $\langle O' \rangle_\pi = \langle O \rangle_\pi$ and, importantly, $\sigma^2(O') < \sigma^2(O)$, as exemplified for atomic forces (under open boundary conditions) in Section C1.

This framework can be extended and generalized beyond forces²⁶ to structural observables such as the one-body density, $\rho(r) \propto \langle \sum_i \delta(r - r_i) \rangle$, and the pair correlation function, $g(r) \propto \langle \sum_{i < j} \delta(r - r_{ij}) \rangle$ ^{27,60–62}, where $r_i = |\mathbf{r}_i|$ and $r_{ij} = |\mathbf{r}_i - \mathbf{r}_j|$. The bare estimators for these quantities are defined by delta function operators, which are notoriously noisy because they probe rare events on thin shells, leading to a systematic bias when implemented in practice via binning. The key step is to choose a vector field \mathbf{A} that is truncated by a Heaviside step function $\theta(s - \xi(\mathbf{r}))$, for an appropriate constraint $\xi(\mathbf{r})$ (for instance $\xi \equiv r_i$ for $\rho(r)$, or $\xi \equiv r_{ij}$ for $g(r)$). Applying the divergence theorem then yields an identity (as detailed in Section C2) that replaces the noisy integration over a shell with an integration over the ball $\{\xi \leq s\}$, inevitably reducing the variance, though at a higher computational cost given the added drift term $\nabla \log \pi$. This latter term is however easily calculated in VMC, where $\pi \propto |\Psi|^2$, and corresponds to the quantum force $\nabla \log \pi = 2\nabla \log \Psi$.

It is worth noting that these ideas have also been developed in the context of classical NVT (classical Monte Carlo and molecular dynamics) simulations⁶⁰, where the Boltzmann distribution $\pi \propto e^{-\beta U}$ is being sampled, and $\nabla_i \log \pi = \beta \mathbf{F}_i^{\text{cl}}$, where β is the inverse temperature and \mathbf{F}_i^{cl} is the classical force on particle i . The resulting force-based estimators for $\rho(r)$ and $g(r)$ have already been shown to lower the variance^{63,64}. We will further exemplify in the Results section the variance reduction for $g(r)$ in VMC, using the following estimator derived in Section C2

$$g(r) \propto \left\langle \sum_{i < j} \theta(r - r_{ij}) \left(\frac{2}{r_{ij}} + \hat{\mathbf{r}}_{ij} \cdot (\mathbf{F}_i - \mathbf{F}_j) \right) \right\rangle, \quad (45)$$

with $\mathbf{F}_i \equiv \nabla_i \log \Psi$ being the quantum force acting on particle i .

Finally, we provide in Section C3 a systematic extension to higher-order correlation functions involving a product of multiple delta functions, for example, angular distribution functions and other multi-constraint structural observables. Such quantities are often calculated in atomistic simulations^{14,65–68}, but the associated bare estimators become increasingly noisy the more delta functions (i.e. constraints) are added. The multi-constraint identity we derive offers an unbiased, variance-reduced alternative that applies not only to VMC/DMC, but also to classical NVT simulations (though, obviously, still at a higher computational cost).

While several of the references mentioned in this section introduce improved estimators for specific observables (mainly for forces, densities and pair correlations), they do not provide a single, systematic formulation that unifies them. In Section C and its subsections, we present such a unified framework explicitly: codimension-0 recovers the familiar zero-mean control variate correction, codimension-1 yields the exact $\delta \rightarrow \theta$ conversion used for $\rho(r)$ and $g(r)$, and codimension-2 extends the construction to products of delta functions. We suspect our formulation could be further generalized and applicable for other observables and cases.

IV. RESULTS

We present VMC results for a periodic system of $N = 128$ hydrogen atoms placed in a cubic cell, with the Hamiltonian taking the usual form given in Eq. (4). We restrict our attention to a single high-pressure configuration at an electronic density of $r_s = 1.19$ (or roughly 650 GPa), where $r_s = a/a_0$, with a and a_0 being the

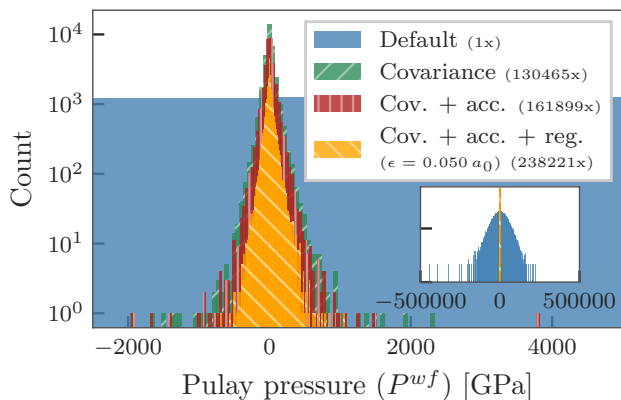


Figure 1. Comparison of Pulay pressure (P^{wf}) estimators for a periodic system of $N = 128$ hydrogen atoms. The estimators’ names and associated variance-reduction factors are reported in the legend. The covariance estimator (denoted also as “Cov.”) is given in Eq. (26), the acceptance trick (denoted as “acc.”) is given in Eq. (28), and the (hard-cutoff) regularized estimator (denoted as “reg.”) is given in Eq. (32).

mean electronic distance and the Bohr radius, respectively. The trial wave function used follows our earlier work¹³, with only minor modifications.

We start by presenting results on the pressure. As previously alluded to in Section II C, the Virial pressure has finite variance and is therefore not challenging to calculate precisely. We therefore only focus on the Pulay pressure contribution, given in Eq. (22). In Fig. 1, we show the importance of the covariance expression given in Eq. (26), improving the variance by five orders of magnitude compared to that of the default estimator. Moreover, we see that applying the acceptance trick (see Eq. (28)) on top – at essentially no additional computational cost – reduces the variance further by a factor of ~ 1.25 . By regularizing this resulting “covariance + acceptance” estimator using a hard-cutoff function, as in Eq. (32), the variance is additionally lowered by a factor of ~ 1.5 . We choose ϵ as the largest value for which the regularized Pulay-pressure mean is statistically indistinguishable from the $\epsilon \rightarrow 0$ reference value (i.e. the residual

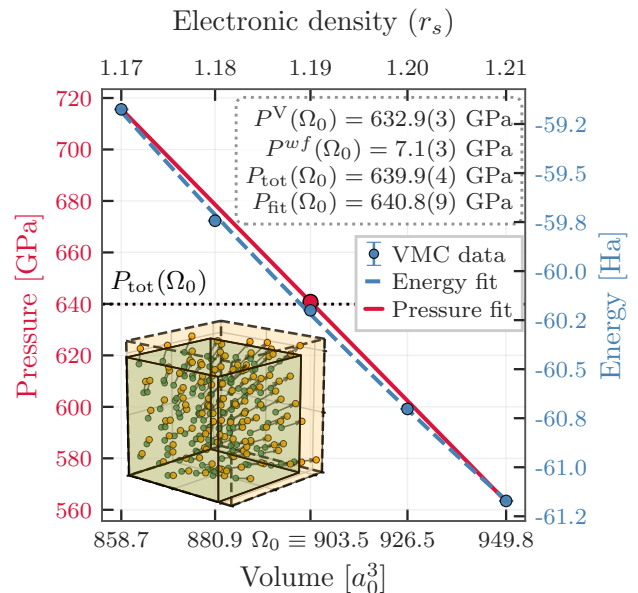


Figure 2. Comparison between the pressure obtained from the direct estimator and from a finite-difference fit. The direct estimate is computed as the sum of the Virial and Pulay contributions, $P_{\text{tot}}(\Omega_0) = P^V(\Omega_0) + P^{wf}(\Omega_0)$ (indicated with a dotted black line), where Ω_0 is the simulation-cell volume of the original (unscaled) nuclear configuration. The finite-difference estimate, denoted $P_{\text{fit}}(\Omega_0)$ (indicated by a large red marker), is obtained by differentiating a polynomial fit to the VMC energy data and evaluating it at Ω_0 . In the inset, the original and scaled cells are shown as light green and light orange surfaces, respectively, with solid and dashed lines marking their boundaries. The scaled configuration is illustrated by displaced nuclear positions; the arrows indicate geometric displacements (not forces). The inset is not to scale and is intended only as a schematic, since the actual volume changes considered are too small to be visible.

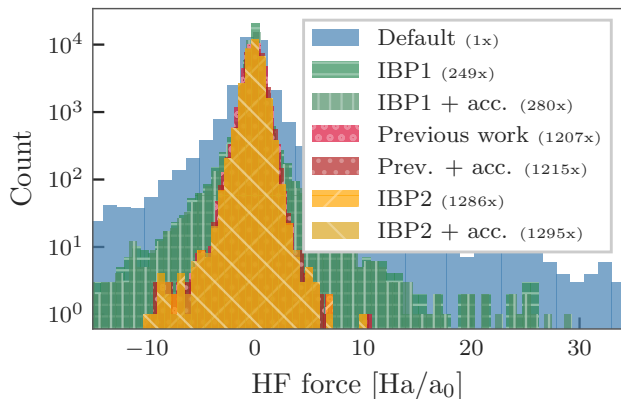


Figure 3. Comparison of the Hellmann-Feynman force estimators. The force component for the proton index 0 in the x -direction is shown without loss of generality. The estimators “IBP1” and “IBP2” are presented in Eqs. (37) and (41), respectively, while “Previous work” (or “Prev.” for short), refers to an estimator suggested in a recent paper²³, that is also described in Section D.

bias is below the error bar), while still yielding clear variance reduction (see Section A 8 for further details). Here $\epsilon = 0.05 a_0$ was systematically chosen. We emphasize that the variance reduction factors reported can change considerably depending on the Monte Carlo configurations sampled and the system considered. Moreover, although the default estimator has formally infinite variance, any finite set of sampled configurations still yields a finite empirical variance, so the reported factors should be understood as finite-sample measures.

To determine the proportion of the Pulay contribution to the total pressure, and simultaneously assess the accuracy of our pressure calculation, we compare with finite difference in Fig. 2. We see that the pressure obtained by direct calculation $P_{\text{tot}}(\Omega_0) = P^V(\Omega_0) + P^{wf}(\Omega_0) = 639.9(4)$ GPa is in agreement with the pressure obtained with finite difference $P_{\text{fit}}(\Omega_0) = 640.8(9)$ GPa, where Ω_0 is the volume of the cell where the original (non-dilated) nuclear configuration is placed. More importantly, although the NQS-based wave function is very good at modeling the ground state (as demonstrated in our earlier work¹³), the Pulay contribution $P^{wf}(\Omega_0) = 7.1(3)$ GPa is non-negligible.

We further note that the NQS-based orbitals have an explicit dependence on the nuclear coordinates \mathbf{R} and on the cell geometry, so the dilation derivative (see Eq. (23)) naturally propagates through the orbitals. This contrasts with the common practice of using DFT orbitals where the \mathbf{R} -dependence is not explicit. There, the orbital response to changes in \mathbf{R} enters implicitly through the Kohn-Sham equations. Neglecting their contributions in the Pulay term will introduce a systematic bias.

Similarly to pressure, atomic forces greatly benefit from variance-reduced estimators. We illustrate this on the same hydrogen system in Fig. 3, where we overlay

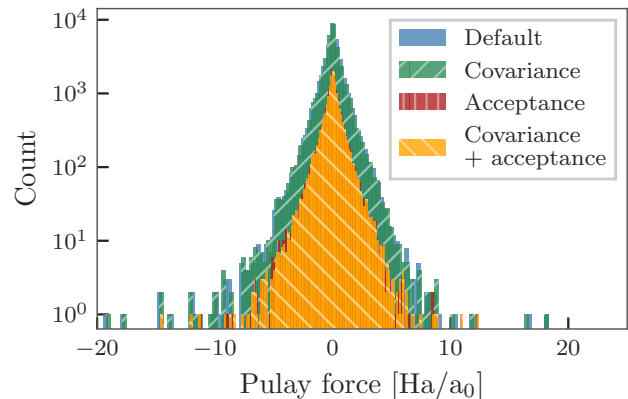


Figure 4. Comparison of the Pulay force estimators. The covariance estimator is given in Eq. (26), and the acceptance trick is given in Eq. (28). The force component for the proton index 0 in the x -direction is shown without loss of generality.

histograms of several Hellmann-Feynman estimators ordered by decreasing variance. The IBP1 estimator introduced in Section III D 1 already suppresses the number of outliers compared with the default estimator, yielding a variance reduction of about two orders of magnitude. This clearly shows how softening the near-coalescence divergence from $\mathcal{O}(1/x^2)$ to $\mathcal{O}(1/x)$ substantially improves the estimator’s reliability. The resolution of the Hellmann-Feynman estimator can be improved further by removing the leading singularity, as outlined in Section III D 2 with the IBP2 estimator, resulting in an additional order of magnitude reduction in variance compared to the default estimator. For comparison, we also include an alternative estimator with a similar variance profile proposed by Qian *et al.*²³. Their construction extends the Assaraf-Caffarel approach²⁶ to periodic systems, following a more heuristic approach. We describe the relation of this estimator to our framework presented in Section III D and provide additional details in Section D. Finally, for all three estimators, applying the acceptance trick on top further reduces the number of outliers and therefore systematically lowers the variance (though to a lesser extent).

In contrast to the Hellmann-Feynman force estimator, the default Pulay force estimator is not noisy, as seen in Fig. 4. While the Pulay force shares the same mathematical structure as the Pulay pressure, that is $F_{I\alpha}^{\text{Pulay}} \propto \langle \Delta E \partial_{R_{I\alpha}} \log \Psi^* \rangle$ and $P^{wf} \propto \langle \Delta E \mathcal{D} \log \Psi^* \rangle$, the difference in variance is influenced by the size and scaling of the derivative operator that multiplies ΔE . In particular, the dilation operator \mathcal{D} acts globally and results in an extensive $\mathcal{O}(N)$ multiplicative factor, as we saw in Eq. (25) for P^{wf} . In comparison, $\partial_{R_{I\alpha}} \log \Psi^*$ describes the response to moving one nucleus, so that its magnitude is typically controlled by the local environment around nucleus I (and importantly does not grow with the system size). As a result, for all estimators

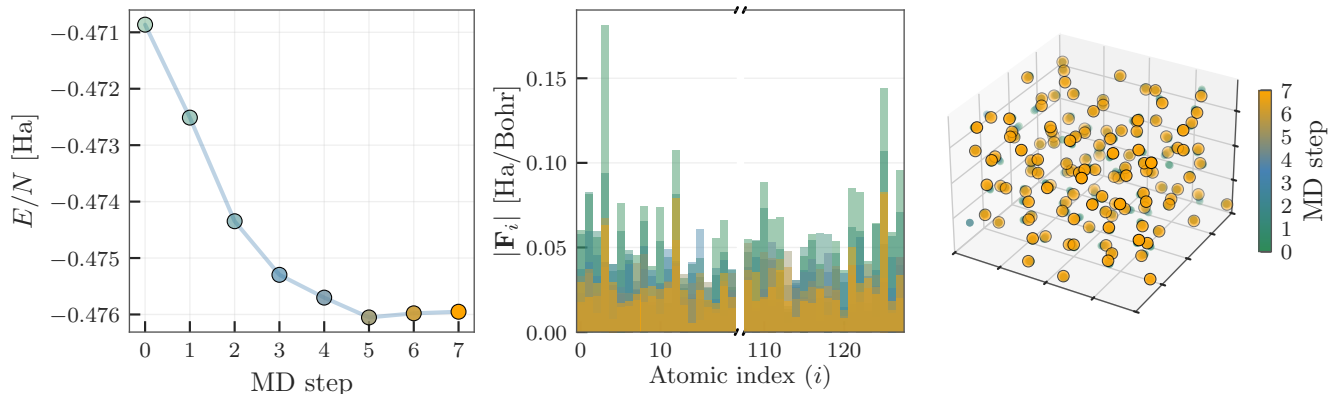


Figure 5. Molecular dynamics evolution of the hydrogen system, showing from left to right the electronic energy, the atomic forces, and the nuclear configurations. The molecular dynamics protocol consists of an iterative three-step procedure: (1) a short VMC optimization; (2) the evaluation of the forces associated with the optimized wave function and nuclear configuration; and (3) the propagation of the nuclear coordinates using the damped velocity Verlet integration scheme based on these forces, after which the cycle is restarted with the updated coordinates.

shown in Fig. 4, the variance reduction factor rounds to 1 (compared to the default estimator), meaning that there is no significant improvement.

As an application of our force estimators, we perform a few molecular dynamics (MD) steps starting from the original hydrogen configuration, using a standard damped velocity Verlet integrator scheme. We report the electronic energy, atomic forces, and nuclear positions along the trajectory in Fig. 5. The MD loop follows a simple three-step protocol, as described in the caption. The total force at each step includes both the Hellmann-Feynman IBP2 and Pulay contributions. Over only five MD steps, the energy decreases by ~ 5 mHa, and the force magnitudes systematically decrease as the nuclei relax.

Because our wave function uses NQS-based orbitals,

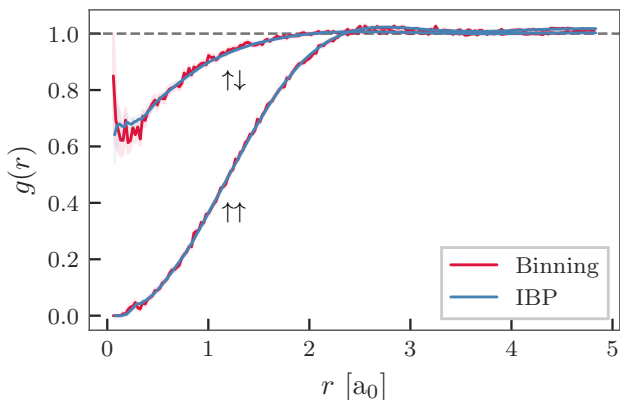


Figure 6. Spin-resolved pair correlation function with the default binning and IBP estimators for a (relatively) small number of Monte Carlo configurations (i.e. 8192). The IBP estimator is defined in Eq. (45).

we can employ transfer learning by initializing each new VMC optimization from the parameters obtained at the previous MD step. As a result, only the first VMC optimization needs to be run in full. Subsequent VMC optimizations typically converge within a few iterations and can be orders of magnitude faster, provided the MD step size is chosen sufficiently small. This contrasts with the common use of fixed DFT orbitals, whose coefficients are tied to a specific nuclear geometry and are generally not transferable across configurations. As noted in the Introduction, this also motivates foundation model wave functions^{15–17}, which could provide accurate forces across many geometries while avoiding re-optimization at each MD step.

As described in Section III E, the integration by parts (IBP) framework extends naturally beyond forces and pressure to other observables. In Fig. 6, we show the spin-resolved electron-electron pair correlation function of the hydrogen configuration, calculated using Eq. (45). For both parallel and anti-parallel spins, the IBP estimator is markedly less noisy than the standard binning estimator and yields a smooth and stable signal, which can generally be achieved with significantly fewer Monte Carlo samples. Its statistical quality is also expected to improve as the radius r increases, since the estimator averages over a ball of radius r , thus enhancing the signal-to-noise ratio. This would be particularly advantageous for systems whose pair-correlation functions exhibit sharp features.

V. CONCLUSION

We have described a set of simple and practical strategies to reduce the variance of force- and pressure-related estimators in variational Monte Carlo. For Pulay-type contributions, we showed that the Metropolis acceptance

trick already regularizes the nodal divergence, reducing the variance from a power-law to a logarithmic one, and that additional regularizations can suppress the residual bias in a controlled manner. For Hellmann-Feynman forces, we derived compact integration-by-parts estimators that remove the Coulomb singularity while remaining straightforward to implement in both open and periodic systems. Beyond their immediate relevance for quantum Monte Carlo calculations, such improved force estimators are also important in a broader context. Indeed, accurate force calculations are increasingly being used as training data for machine-learned interatomic force fields, which in turn enable large-scale classical and path-integral molecular dynamics simulations^{66,69–71}.

We also showed that the same perspective extends beyond forces and pressure. In particular, the divergence-theorem identities introduced here provide a route to variance-reduced estimators for other observables, including pair correlations and angular distribution functions, by using zero-mean control variates or replacing shell integrals (delta functions) to volume integrals (Heaviside step functions).

A key practical point is that all of these improvements are compatible with standard VMC workflows and incur little additional computational cost. These can be combined with flexible trial wave functions, such as NQS, where accurate forces and pressure are increasingly important for equations-of-state calculations and structural optimization, for instance.

Looking ahead, it would be natural to extend the same ideas to other observables involving wave function derivatives, such as higher-order response properties or the stress tensor in periodic systems^{72–74}. Combined with transferable or foundation model wave functions, these methods can be naturally extended to fixed-pressure calculations^{12,68}, enabling the minimization of the Gibbs free energy for determining atomic structures and cell geometries in materials.

ACKNOWLEDGMENTS

We thank D. Ceperley, C. Pierleoni, Y. Yang, K. Nakano, and G. Mazzola for useful discussions and for providing reference data for comparisons. The authors acknowledge support from SEFRI under Grant No. MB22.00051 (NEQS - Neural Quantum Simulation) and from the French Agency for Research, project SIX (ANR-23-CE30-0022).

REFERENCES

- ¹R. P. Feynman, “Forces in molecules,” *Phys. Rev.* **56**, 340–343 (1939).
- ²P. Pulay, “Ab initio calculation of force constants and equilibrium geometries in polyatomic molecules,” *Molecular Physics* **17**, 197–204 (1969).
- ³O. H. Nielsen and R. M. Martin, “First-principles calculation of stress,” *Phys. Rev. Lett.* **50**, 697–700 (1983).
- ⁴O. H. Nielsen and R. M. Martin, “Quantum-mechanical theory of stress and force,” *Phys. Rev. B* **32**, 3780–3791 (1985).
- ⁵J. S. Spencer, D. Pfau, A. Botev, and W. M. C. Foulkes, “Better, faster fermionic neural networks,” (2020), [arXiv:2011.07125 \[physics.comp-ph\]](https://arxiv.org/abs/2011.07125).
- ⁶J. Hermann, Z. Schätzle, and F. Noé, “Deep-neural-network solution of the electronic schrödinger equation,” *Nature Chemistry* **12**, 891–897 (2020).
- ⁷G. Cassella, H. Sutterud, S. Azadi, N. D. Drummond, D. Pfau, J. S. Spencer, and W. M. C. Foulkes, “Discovering quantum phase transitions with fermionic neural networks,” *Phys. Rev. Lett.* **130**, 036401 (2023).
- ⁸M. Wilson, S. Moroni, M. Holzmann, N. Gao, F. Wudarski, T. Vegge, and A. Bhowmik, “Neural network ansatz for periodic wave functions and the homogeneous electron gas,” *Phys. Rev. B* **107**, 235139 (2023).
- ⁹G. Pescia, J. Nys, J. Kim, A. Lovato, and G. Carleo, “Message-passing neural quantum states for the homogeneous electron gas,” *Phys. Rev. B* **110**, 035108 (2024).
- ¹⁰J. Kim, G. Pescia, B. Fore, J. Nys, G. Carleo, S. Gandolfi, M. Hjorth-Jensen, and A. Lovato, “Neural-network quantum states for ultra-cold fermi gases,” *Communications Physics* **7**, 148 (2024).
- ¹¹C. Smith, Y. Chen, R. Levy, Y. Yang, M. A. Morales, and S. Zhang, “Unified variational approach description of ground-state phases of the two-dimensional electron gas,” *Phys. Rev. Lett.* **133**, 266504 (2024).
- ¹²D. Linteau, G. Pescia, J. Nys, G. Carleo, and M. Holzmann, “Phase diagram and crystal melting of helium-4 in two dimensions,” *Phys. Rev. Lett.* **134**, 246001 (2025).
- ¹³D. Linteau, S. Moroni, G. Carleo, and M. Holzmann, “Neural wave functions for high-pressure atomic hydrogen,” (2025), [arXiv:2504.07062 \[cond-mat.str-el\]](https://arxiv.org/abs/2504.07062).
- ¹⁴C. Smith, Y. Yang, Z.-Q. Wan, Y. Chen, M. A. Morales, and S. Zhang, “Neural network discovery of paired wigner crystals in artificial graphene,” (2026), [arXiv:2602.16798 \[quant-ph\]](https://arxiv.org/abs/2602.16798).
- ¹⁵M. Scherbela, L. Gerard, and P. Grohs, “Towards a transferable fermionic neural wavefunction for molecules,” *Nature Communications* **15**, 120 (2024).
- ¹⁶N. Gao and S. Günemann, “Neural pfaiffians: Solving many many-electron schrödinger equations,” (2024), [arXiv:2405.14762 \[cs.LG\]](https://arxiv.org/abs/2405.14762).
- ¹⁷R. Rende, L. L. Viteritti, F. Becca, A. Scardicchio, A. Laio, and G. Carleo, “Foundation neural-networks quantum states as a unified ansatz for multiple hamiltonians,” *Nature Communications* **16**, 7213 (2025).
- ¹⁸J. van Rhijn, C. Filippi, S. De Palo, and S. Moroni, “Energy derivatives in real-space diffusion monte carlo,” *Journal of Chemical Theory and Computation* **18**, 118–123 (2022), PMID: 34930005.
- ¹⁹E. Sloatman, I. Poltavsky, R. Shinde, J. Cocomello, S. Moroni, A. Tkatchenko, and C. Filippi, “Accurate quantum monte carlo forces for machine-learned force fields: Ethanol as a benchmark,” *Journal of Chemical Theory and Computation* **20**, 6020–6027 (2024).
- ²⁰M. H. Kalos and P. A. Whitlock, *Monte Carlo Methods*, 2nd ed. (Wiley-VCH, 2008).
- ²¹C. J. Umrigar, “Two aspects of quantum monte carlo: Determination of accurate wavefunctions and determination of potential energy surfaces of molecules,” *International Journal of Quantum Chemistry* **36**, 217–230 (1989).
- ²²C. Filippi and C. J. Umrigar, “Correlated sampling in quantum monte carlo: A route to forces,” *Phys. Rev. B* **61**, R16291–R16294 (2000).
- ²³Y. Qian, X. Li, and J. Chen, “Force and stress calculations with a neural-network wave function for solids,” *Faraday Discuss.* **254**, 529–541 (2024).

- ²⁴R. Assaraf and M. Caffarel, “Zero-variance principle for monte carlo algorithms,” *Phys. Rev. Lett.* **83**, 4682–4685 (1999).
- ²⁵R. Assaraf and M. Caffarel, “Computing forces with quantum monte carlo,” *The Journal of Chemical Physics* **113**, 4028–4034 (2000).
- ²⁶R. Assaraf and M. Caffarel, “Zero-variance zero-bias principle for observables in quantum monte carlo: Application to forces,” *The Journal of Chemical Physics* **119**, 10536–10552 (2003).
- ²⁷J. Toulouse, R. Assaraf, and C. J. Umrigar, “Zero-variance zero-bias quantum monte carlo estimators of the spherically and system-averaged pair density,” *The Journal of Chemical Physics* **126**, 244112 (2007).
- ²⁸S. Chiesa, D. M. Ceperley, and S. Zhang, “Accurate, efficient, and simple forces computed with quantum monte carlo methods,” *Phys. Rev. Lett.* **94**, 036404 (2005).
- ²⁹D. M. Ceperley and B. Bernu, “The calculation of excited state properties with quantum monte carlo,” *The Journal of Chemical Physics* **89**, 6316–6328 (1988).
- ³⁰C. Attaccalite and S. Sorella, “Stable liquid hydrogen at high pressure by a novel ab initio molecular-dynamics calculation,” *Phys. Rev. Lett.* **100**, 114501 (2008).
- ³¹A. Misery, L. Gravina, A. Santini, and F. Vicentini, “Looking elsewhere: improving variational monte carlo gradients by importance sampling,” *Machine Learning: Science and Technology* **7**, 015035 (2026).
- ³²S. Pathak and L. K. Wagner, “A light weight regularization for wave function parameter gradients in quantum monte carlo,” *AIP Advances* **10**, 085213 (2020).
- ³³J. R. Trail, “Heavy-tailed random error in quantum monte carlo,” *Phys. Rev. E* **77**, 016703 (2008).
- ³⁴J. R. Trail, “Alternative sampling for variational quantum monte carlo,” *Phys. Rev. E* **77**, 016704 (2008).
- ³⁵P. L. Ríos and G. J. Conduit, “Tail-regression estimator for heavy-tailed distributions of known tail indices and its application to continuum quantum monte carlo data,” *Phys. Rev. E* **99**, 063312 (2019).
- ³⁶D. Ceperley, G. V. Chester, and M. H. Kalos, “Monte carlo simulation of a many-fermion study,” *Phys. Rev. B* **16**, 3081–3099 (1977).
- ³⁷G. Carleo, F. Becca, M. Schiró, and M. Fabrizio, “Localization and glassy dynamics of many-body quantum systems,” *Scientific Reports* **2**, 243 (2012).
- ³⁸G. Carleo, L. Cevolani, L. Sanchez-Palencia, and M. Holzmann, “Unitary dynamics of strongly interacting bose gases with the time-dependent variational monte carlo method in continuous space,” *Phys. Rev. X* **7**, 031026 (2017).
- ³⁹M. Schmitt and M. Heyl, “Quantum many-body dynamics in two dimensions with artificial neural networks,” *Phys. Rev. Lett.* **125**, 100503 (2020).
- ⁴⁰R. Verdel, M. Schmitt, Y.-P. Huang, P. Karpov, and M. Heyl, “Variational classical networks for dynamics in interacting quantum matter,” *Phys. Rev. B* **103**, 165103 (2021).
- ⁴¹A. Sinibaldi, C. Giuliani, G. Carleo, and F. Vicentini, “Unbiasing time-dependent Variational Monte Carlo by projected quantum evolution,” *Quantum* **7**, 1131 (2023).
- ⁴²J. Nys, Z. Denis, and G. Carleo, “Real-time quantum dynamics of thermal states with neural thermofields,” *Phys. Rev. B* **109**, 235120 (2024).
- ⁴³L. Gravina, V. Savona, and F. Vicentini, “Neural Projected Quantum Dynamics: a systematic study,” *Quantum* **9**, 1803 (2025).
- ⁴⁴H. Shi and S. Zhang, “Infinite variance in fermion quantum monte carlo calculations,” *Phys. Rev. E* **93**, 033303 (2016).
- ⁴⁵Z.-Q. Wan and S. Zhang, “Addressing the infinite variance problem in fermionic monte carlo simulations: Retrospective error remediation and the exact bridge link method,” *Phys. Rev. E* **112**, 065309 (2025).
- ⁴⁶P. P. Ewald, “Die berechnung optischer und elektrostatischer gitterpotentiale,” *Annalen der Physik* **369**, 253–287 (1921).
- ⁴⁷F. Delyon, B. Bernu, and M. Holzmann, “Confidence and efficiency scaling in variational quantum monte carlo calculations,” *Phys. Rev. E* **95**, 023307 (2017).
- ⁴⁸S. Sorella, “Wave function optimization in the variational monte carlo method,” *Phys. Rev. B* **71**, 241103 (2005).
- ⁴⁹C. J. Umrigar and C. Filippi, “Energy and variance optimization of many-body wave functions,” *Phys. Rev. Lett.* **94**, 150201 (2005).
- ⁵⁰C. R. Rao, “Information and the accuracy attainable in the estimation of statistical parameters,” *Bulletin of the Calcutta Mathematical Society* **37**, 81–91 (1945).
- ⁵¹D. Blackwell, “Conditional expectation and unbiased sequential estimation,” *The Annals of Mathematical Statistics* **18**, 105 – 110 (1947).
- ⁵²G. Casella and C. P. Robert, “Rao-blackwellisation of sampling schemes,” *Biometrika* **83**, 81–94 (1996).
- ⁵³C. Stein, “A bound for the error in the normal approximation to the distribution of a sum of dependent random variables,” in *Proceedings of the Sixth Berkeley Symposium on Mathematical Statistics and Probability, Volume 2: Probability Theory*, edited by L. M. Le Cam, J. Neyman, and E. L. Scott (University of California Press, Berkeley, CA, 1972) pp. 583–602.
- ⁵⁴A. D. Barbour, “Stein’s method and poisson process convergence,” *Journal of Applied Probability* **25**, 175–184 (1988).
- ⁵⁵A. D. Barbour, “Stein’s method for diffusion approximations,” *Probability Theory and Related Fields* **84**, 297–322 (1990).
- ⁵⁶J. Gorham and L. Mackey, “Measuring sample quality with Stein’s method,” in *Advances in Neural Information Processing Systems 28 (NeurIPS)*, edited by C. Cortes, N. D. Lawrence, D. D. Lee, M. Sugiyama, and R. Garnett (Curran Associates, Inc., 2015) pp. 226–234.
- ⁵⁷J. Gorham and L. Mackey, “Measuring sample quality with kernels,” in *Proceedings of the 34th International Conference on Machine Learning (ICML)*, Proceedings of Machine Learning Research, Vol. 70 (PMLR, 2017) pp. 1292–1301.
- ⁵⁸C. J. Oates, M. Girolami, and N. Chopin, “Control functionals for monte carlo integration,” *Journal of the Royal Statistical Society: Series B (Statistical Methodology)* **79**, 695–718 (2017).
- ⁵⁹S. Si, C. J. Oates, A. B. Duncan, L. Carin, and F.-X. Briol, “Scalable control variates for monte carlo methods via stochastic optimization,” in *Monte Carlo and Quasi-Monte Carlo Methods*, edited by A. Keller (Springer International Publishing, Cham, 2022) pp. 205–221.
- ⁶⁰A. B. Adib and C. Jarzynski, “Unbiased estimators for spatial distribution functions of classical fluids,” *The Journal of Chemical Physics* **122**, 014114 (2004).
- ⁶¹R. Assaraf, M. Caffarel, and A. Scemama, “Improved monte carlo estimators for the one-body density,” *Phys. Rev. E* **75**, 035701 (2007).
- ⁶²M. C. Per, S. P. Russo, and I. K. Snook, “Anisotropic intracule densities and electron correlation in h₂: A quantum monte carlo study,” *The Journal of Chemical Physics* **130**, 134103 (2009).
- ⁶³D. Borgis, R. Assaraf, B. Rotenberg, and R. Vuilleumier, “Computation of pair distribution functions and three-dimensional densities with a reduced variance principle,” *Molecular Physics* **111**, 3486–3492 (2013).
- ⁶⁴B. Rotenberg, “Use the force! reduced variance estimators for densities, radial distribution functions, and local mobilities in molecular simulations,” *The Journal of Chemical Physics* **153**, 150902 (2020).
- ⁶⁵J. DiStasio, Robert A., B. Santra, Z. Li, X. Wu, and R. Car, “The individual and collective effects of exact exchange and dispersion interactions on the ab initio structure of liquid water,” *The Journal of Chemical Physics* **141**, 084502 (2014).
- ⁶⁶H. Niu, Y. Yang, S. Jensen, M. Holzmann, C. Pierleoni, and D. M. Ceperley, “Stable solid molecular hydrogen above 900 K from a machine-learned potential trained with diffusion quantum monte carlo,” *Phys. Rev. Lett.* **130**, 076102 (2023).
- ⁶⁷M. Istas, S. Jensen, Y. Yang, M. Holzmann, C. Pierleoni, and D. M. Ceperley, “Liquid-liquid phase transition of hydrogen

- and its critical point: Analysis from ab initio simulation and a machine-learned potential.” *Phys. Rev. E* **111**, 045307 (2025).
- ⁶⁸S. Chai, C. Lin, X. Dong, Y. Li, W. Ouyang, L. Wang, and X. C. Xie, “Revisiting the broken symmetry phase of solid hydrogen: A neural network variational monte carlo study,” (2025), [arXiv:2512.17703 \[cond-mat.str-el\]](https://arxiv.org/abs/2512.17703).
- ⁶⁹D. M. Ceperley, S. Jensen, Y. Yang, H. Niu, C. Pierleoni, and M. Holzmann, “Training models using forces computed by stochastic electronic structure methods,” *Electronic Structure* **6**, 015011 (2024).
- ⁷⁰C. Huang and B. M. Rubenstein, “Machine learning diffusion monte carlo forces,” *The Journal of Physical Chemistry A* **127**, 339–355 (2023).
- ⁷¹G. Tenti, K. Nakano, and M. Casula, “Self-consistency error correction for accurate machine learning potentials from variational monte carlo,” *Journal of Chemical Theory and Computation* **21**, 9335–9346 (2025).
- ⁷²K. Nakano, T. Morresi, M. Casula, R. Maezono, and S. Sorella, “Atomic forces by quantum monte carlo: Application to phonon dispersion calculations,” *Phys. Rev. B* **103**, L121110 (2021).
- ⁷³S. Chen and S. Zhang, “Computation of forces and stresses in solids: Towards accurate structural optimization with auxiliary-field quantum monte carlo,” *Phys. Rev. B* **107**, 195150 (2023).
- ⁷⁴S. Zhang, R. Paul, S. X. Hu, and M. A. Morales, “Toward an accurate equation of state and b1-b2 phase boundary for magnesium oxide up to terapascal pressures and electron-volt temperatures,” *Phys. Rev. B* **107**, 224109 (2023).

SUPPLEMENTAL MATERIAL

Appendix A: Near-node scaling of regularized acceptance-based Pulay estimators

In this appendix, we analyze the near-node scaling of several estimators for Pulay-type observables. We first introduce some notation and assumptions used throughout the section, then derive the variance of the default estimator, of the acceptance-based estimator, and of its regularized forms. We finally discuss the bias introduced by the latter and how it can be systematically reduced by smooth cutoff functions.

1. Nodal surface preliminaries

We consider an observable $O(\mathbf{r})$ sampled in VMC from the stationary distribution $\pi(\mathbf{r}) = |\Psi(\mathbf{r})|^2$. Throughout this appendix, \mathbf{r}_i denotes the current configuration of the Markov chain and \mathbf{r}_f the proposed configuration. Expectations over $(\mathbf{r}_i, \mathbf{r}_f)$ are understood as

$$\langle \cdots \rangle = \int d\mathbf{r}_i \pi(\mathbf{r}_i) \int d\mathbf{r}_f p(\mathbf{r}_f | \mathbf{r}_i) (\cdots), \quad (\text{A1})$$

where $p(\mathbf{r}_f | \mathbf{r}_i)$ is the proposal distribution. For simplicity, and without loss of generality for the present scaling arguments, we assume a symmetric proposal, $p(\mathbf{x} | \mathbf{y}) = p(\mathbf{y} | \mathbf{x})$, so that the Metropolis-Hastings acceptance probability reduces to

$$a(\mathbf{r}_i \rightarrow \mathbf{r}_f) = \min \left(1, \frac{|\Psi(\mathbf{r}_f)|^2}{|\Psi(\mathbf{r}_i)|^2} \right). \quad (\text{A2})$$

We also assume that $p(\mathbf{r}_f | \mathbf{r}_i)$ is smooth and non-zero in the vicinity of the nodal surface, so that it only contributes finite pre-factors to the asymptotic scalings presented below. We denote the nodal surface as

$$\mathcal{N} = \{\mathbf{r} \in \mathbb{R}^{3N} | \Psi(\mathbf{r}) = 0\}. \quad (\text{A3})$$

Close to a generic point on \mathcal{N} , we introduce local coordinates $\mathbf{r} = (\xi, \mathbf{r}_{\parallel})$, where $\xi \in \mathbb{R}$ is the signed distance to the node and $\mathbf{r}_{\parallel} \in \mathbb{R}^{3N-1}$ parameterizes the nodal surface. Assuming the derivative along the normal direction does not vanish, i.e. $\Phi(\mathbf{r}_{\parallel}) \equiv \partial_{\xi} \Psi(\xi, \mathbf{r}_{\parallel})|_{\xi=0} \neq 0$, a first-order Taylor expansion along that direction gives

$$\Psi(\xi, \mathbf{r}_{\parallel}) = \Phi(\mathbf{r}_{\parallel})\xi + \mathcal{O}(\xi^2), \quad (\text{A4})$$

so that

$$|\Psi(\xi, \mathbf{r}_{\parallel})|^2 = |\Phi(\mathbf{r}_{\parallel})|^2 \xi^2 + \mathcal{O}(|\xi|^3) \sim \xi^2. \quad (\text{A5})$$

For Pulay-type observables,

$$O(\mathbf{r}) \equiv (E_L(\mathbf{r}) - E) \partial_p \log \Psi^*(\mathbf{r}), \quad (\text{A6})$$

one generically has near the node

$$E_L(\mathbf{r}) \sim \xi^{-1}, \quad \partial_p \log \Psi^*(\mathbf{r}) \sim \xi^{-1}, \quad O(\mathbf{r}) \sim \xi^{-2}. \quad (\text{A7})$$

Since we are only interested in the leading near-node scaling, and the two sides of the nodal surface differ only by finite prefactors, we restrict the analysis to $\xi > 0$. The tangential integrals over \mathbf{r}_{\parallel} remain finite and only contribute overall constants, so from now on we keep track only of the normal coordinate $\xi > 0$. We denote by ξ_0 a fixed microscopic scale delimiting the region where the nodal expansion is valid, and by ξ_c (with $\xi_c \ll \xi_0$) a formal short-distance cutoff used only to display the divergence of unregularized estimators.

2. Default estimator: power-law divergent variance

For the default estimator $O(\mathbf{r}) \sim \xi^{-2}$, the mean remains finite because

$$\langle O \rangle \sim \int_0^{\xi_0} d\xi |\Psi|^2 O \sim \int_0^{\xi_0} d\xi \xi^2 \xi^{-2}, \quad (\text{A8})$$

which is integrable at $\xi = 0$. By contrast, the second moment behaves as

$$\langle O^2 \rangle \sim \int_{\xi_c}^{\xi_0} d\xi \xi^2 \xi^{-4} = \int_{\xi_c}^{\xi_0} d\xi \xi^{-2} = \frac{1}{\xi_c} - \frac{1}{\xi_0} \sim \xi_c^{-1}. \quad (\text{A9})$$

Therefore the default Pulay estimator has a power-law divergent variance,

$$\boxed{\text{Var}(O) \sim \xi_c^{-1}}. \quad (\text{A10})$$

3. Acceptance-based estimator

The acceptance trick replaces $O(\mathbf{r})$ by the conditional estimator

$$\tilde{O}(\mathbf{r}_i, \mathbf{r}_f) = a(\mathbf{r}_i \rightarrow \mathbf{r}_f) O(\mathbf{r}_f) + [1 - a(\mathbf{r}_i \rightarrow \mathbf{r}_f)] O(\mathbf{r}_i). \quad (\text{A11})$$

This estimator is unbiased, as previously discussed under Eq. (28). Near the node, the acceptance probability scales as $a(\mathbf{r}_i \rightarrow \mathbf{r}_f) \sim \min(1, \xi_f^2/\xi_i^2)$. It is therefore natural to split the (ξ_i, ξ_f) plane into the two regions

$$\text{(A)} \quad \xi_f \geq \xi_i, \quad \text{(B)} \quad \xi_f < \xi_i. \quad (\text{A12})$$

In region (A), one has $a = 1$, so $\tilde{O} \sim O(\xi_f) \sim \xi_f^{-2}$ and therefore

$$\langle \tilde{O}^2 \rangle_A \sim \int_{\xi_c}^{\xi_0} d\xi_i \xi_i^2 \int_{\xi_i}^{\xi_0} d\xi_f \xi_f^{-4} \sim \int_{\xi_c}^{\xi_0} d\xi_i \xi_i^2 \xi_i^{-3} = \int_{\xi_c}^{\xi_0} d\xi_i \xi_i^{-1}. \quad (\text{A13})$$

In region (B), one has $a \sim \xi_f^2/\xi_i^2$, hence $aO(\xi_f) \sim \xi_i^{-2}$ and $(1-a)O(\xi_i) \sim \xi_i^{-2}$, so $\tilde{O} \sim \xi_i^{-2}$. This gives

$$\langle \tilde{O}^2 \rangle_B \sim \int_{\xi_c}^{\xi_0} d\xi_i \xi_i^2 \int_0^{\xi_i} d\xi_f \xi_i^{-4} \sim \int_{\xi_c}^{\xi_0} d\xi_i \xi_i^2 \xi_i \xi_i^{-4} = \int_{\xi_c}^{\xi_0} d\xi_i \xi_i^{-1}. \quad (\text{A14})$$

In both regions, we obtain the logarithmic divergence

$$\boxed{\text{Var}(\tilde{O}) \sim \log\left(\frac{\xi_0}{\xi_c}\right)}. \quad (\text{A15})$$

Thus the acceptance trick weakens the variance divergence from power-law to logarithmic.

4. Hard-cutoff regularizations of the acceptance estimator

A simple way to make the variance finite for any fixed $\epsilon > 0$ is to multiply the acceptance estimator by a cutoff that removes a neighborhood of the nodal surface. Two natural choices are

$$\tilde{O}_\epsilon^{(1)}(\mathbf{r}_i, \mathbf{r}_f) = \theta_\epsilon(\xi_i) \tilde{O}(\mathbf{r}_i, \mathbf{r}_f), \quad (\text{A16})$$

and

$$\tilde{O}_\epsilon^{(2)}(\mathbf{r}_i, \mathbf{r}_f) = \Theta_\epsilon(\xi_i, \xi_f) \tilde{O}(\mathbf{r}_i, \mathbf{r}_f), \quad (\text{A17})$$

where

$$\theta_\epsilon(\xi) = \begin{cases} 0, & 0 \leq \xi < \epsilon, \\ 1, & \xi \geq \epsilon, \end{cases} \quad \Theta_\epsilon(\xi_i, \xi_f) = \begin{cases} 0, & 0 \leq \xi_i < \epsilon \text{ and } 0 \leq \xi_f < \epsilon, \\ 1, & \text{otherwise,} \end{cases} \quad (\text{A18})$$

or equivalently, using the step function $\theta_\epsilon(\xi)$ to define Θ_ϵ gives $\Theta_\epsilon(\xi_i, \xi_f) = 1 - [1 - \theta_\epsilon(\xi_i)][1 - \theta_\epsilon(\xi_f)]$. The first excludes all samples whose current point lies within distance ϵ of the node. The second is more selective and excludes only proposals for which both the current and proposed points lie in the ‘‘nodal square’’ $\{0 < \xi_i < \epsilon\} \cup \{0 < \xi_f < \epsilon\}$.

a. Variance

For $\tilde{O}_\epsilon^{(1)}$, the lower bound of the ξ_i integral is simply shifted from ξ_c to ϵ , so

$$\text{Var} \left(\tilde{O}_\epsilon^{(1)} \right) \sim \log \left(\frac{\xi_0}{\epsilon} \right). \quad (\text{A19})$$

For $\tilde{O}_\epsilon^{(2)}$, the square $0 < \xi_i < \epsilon$, $0 < \xi_f < \epsilon$ is excluded. In region (A), the lower bound of the ξ_f -integral becomes $\max(\xi_i, \epsilon)$, so

$$\langle (\tilde{O}_\epsilon^{(2)})^2 \rangle_A \sim \int_0^{\xi_0} d\xi_i \xi_i^2 \int_{\max(\xi_i, \epsilon)}^{\xi_0} d\xi_f \xi_f^{-4}. \quad (\text{A20})$$

Splitting the outer integral into $0 < \xi_i < \epsilon$ and $\epsilon < \xi_i < \xi_0$, one finds that the former contributes only a finite constant, whereas the latter gives the same logarithm as before. In region (B), the inequality $0 < \xi_f < \xi_i$ holds. Therefore, if $\xi_i < \epsilon$, then necessarily $\xi_f < \epsilon$ as well, so the pair (ξ_i, ξ_f) lies inside the square removed by Θ_ϵ . Hence the condition $\Theta_\epsilon = 1$ forces $\xi_i > \epsilon$, and the contribution from region (B) starts at ϵ , yielding once again $\int_\epsilon^{\xi_0} d\xi_i \xi_i^{-1}$. Hence

$$\text{Var} \left(\tilde{O}_\epsilon^{(2)} \right) \sim \log \left(\frac{\xi_0}{\epsilon} \right). \quad (\text{A21})$$

b. Bias

For a regularized observable O_ϵ , targeting the associated default observable O , we define its bias with respect to the exact expectation value $\langle O \rangle$ as

$$\text{Bias}(O_\epsilon) \equiv \langle O_\epsilon \rangle - \langle O \rangle. \quad (\text{A22})$$

Since the (unregularized) acceptance estimator is unbiased, the bias of the hard-cutoff estimators is simply the contribution removed by the cutoff.

For $\tilde{O}_\epsilon^{(1)}$, the contribution removed comes from $0 < \xi_i < \epsilon$:

$$\text{Bias} \left(\tilde{O}_\epsilon^{(1)} \right) \sim \int_0^\epsilon d\xi_i \xi_i^2 \left[\int_{\xi_i}^{\xi_0} d\xi_f \xi_f^{-2} + \int_0^{\xi_i} d\xi_f \xi_i^{-2} \right]. \quad (\text{A23})$$

The first term corresponds to region (A), where $a = 1$ and $\tilde{O} \sim \xi_f^{-2}$, while the second corresponds to region (B), where $\tilde{O} \sim \xi_i^{-2}$. Since $\int_{\xi_i}^{\xi_0} d\xi_f \xi_f^{-2} \sim \xi_i^{-1}$ and $\int_0^{\xi_i} d\xi_f \xi_i^{-2} \sim \xi_i^{-1}$, one finds

$$\boxed{\text{Bias}(\tilde{O}_\epsilon^{(1)}) = \mathcal{O}(\epsilon^2)}. \quad (\text{A24})$$

For the more selective cutoff $\tilde{O}_\epsilon^{(2)}$, the removed contribution is restricted to the square $0 < \xi_i < \epsilon$ and $0 < \xi_f < \epsilon$, so that

$$\text{Bias}(\tilde{O}_\epsilon^{(2)}) \sim \int_0^\epsilon d\xi_i \xi_i^2 \left[\int_{\xi_i}^\epsilon d\xi_f \xi_f^{-2} + \int_0^{\xi_i} d\xi_f \xi_i^{-2} \right], \quad (\text{A25})$$

where the first and second terms correspond to regions (A) and (B), respectively. Therefore, both contributions scale as $\int_0^\epsilon d\xi_i \xi_i$, yielding

$$\boxed{\text{Bias}(\tilde{O}_\epsilon^{(2)}) = \mathcal{O}(\epsilon^2)}, \quad (\text{A26})$$

though with a smaller prefactor as compared to $\tilde{O}_\epsilon^{(1)}$, so $\text{Bias}(\tilde{O}_\epsilon^{(2)}) < \text{Bias}(\tilde{O}_\epsilon^{(1)})$. This is obviously because $\tilde{O}_\epsilon^{(1)}$ discards all points with $0 < \xi_i < \epsilon$, independently of ξ_f , excluding the entire strip $\{0 < \xi_i < \epsilon\} \cup \{0 < \xi_f < \xi_0\}$, while $\tilde{O}_\epsilon^{(2)}$ discards “only” the square $\{0 < \xi_i < \epsilon\} \cup \{0 < \xi_f < \epsilon\}$.

5. Smooth cutoffs and systematic cancellation of the bias

The quadratic bias of a hard cutoff is not fundamental. It arises because the leading contribution removed from the nodal strip is linear in the distance to the node (i.e. $\text{Bias} \sim \int_0^\epsilon \xi d\xi \sim \epsilon^2$). This can be changed by replacing the sharp cutoff by a smooth function³². We consider

$$\hat{O}_\epsilon(\mathbf{r}_i, \mathbf{r}_f) = \chi_\epsilon(\xi_i) \tilde{O}(\mathbf{r}_i, \mathbf{r}_f), \quad \text{where} \quad \chi_\epsilon(\xi) = \begin{cases} \chi(\xi/\epsilon), & 0 \leq \xi < \epsilon, \\ 1, & \xi \geq \epsilon, \end{cases} \quad (\text{A27})$$

for some function $\chi : [0, 1] \rightarrow \mathbb{R}$ such that $\chi(0) = 0$ and $\chi(1) = 1$. We may additionally impose smooth matching conditions such as $\chi'(0) = 0$ and $\chi'(1) = 0$. (The generalization to a two-point smooth cutoff estimator $\hat{O}_\epsilon^{(2)}(\mathbf{r}_i, \mathbf{r}_f) = \varphi_\epsilon(\xi_i, \xi_f) \tilde{O}(\mathbf{r}_i, \mathbf{r}_f)$, for some smooth cutoff function φ_ϵ , will not be pursued here.)

To analyze the bias, we define the following contribution to the mean of the acceptance estimator by

$$G(\xi_i) \equiv \int d\mathbf{r}_{i,\parallel} \int d\mathbf{r}_f |\Psi(\mathbf{r}_i)|^2 p(\mathbf{r}_f | \mathbf{r}_i) \tilde{O}(\mathbf{r}_i, \mathbf{r}_f), \quad (\text{A28})$$

where $\mathbf{r}_i = (\xi_i, \mathbf{r}_{i,\parallel})$ and $\xi_i > 0$. In other words, $G(\xi_i)$ is the contribution to the expectation value of the acceptance-based estimator after integrating out all tangential coordinates and the proposed configuration \mathbf{r}_f , while keeping fixed the normal distance ξ_i of the current configuration to the nodal surface.

We saw for the hard-cutoff bias analysis that the contribution removed from the strip scales like $\int_0^\epsilon d\xi_i G(\xi_i) \sim \epsilon^2$. For that to happen, $G(\xi_i)$ itself must scale linearly at leading order, that is, $G(\xi_i) \sim \xi_i$. Assuming G is smooth enough near $\xi_i = 0$, its Taylor expansion is

$$G(\xi_i) = c_1 \xi_i + c_2 \xi_i^2 + \mathcal{O}(\xi_i^3) = \sum_{n \geq 1} c_n \xi_i^n. \quad (\text{A29})$$

The analogous expression of the $\tilde{O}_\epsilon^{(1)}$ -bias given in Eq. (A23) for the smooth-cutoff estimator \hat{O}_ϵ is then

$$\text{Bias}(\hat{O}_\epsilon) = \int_0^\epsilon d\xi [\chi(\xi/\epsilon) - 1] G(\xi). \quad (\text{A30})$$

Introducing $t = \xi/\epsilon$, so $d\xi = \epsilon dt$, we obtain

$$\begin{aligned} \text{Bias}(\widehat{O}_\epsilon) &= \int_0^\epsilon d\xi [\chi(\xi/\epsilon) - 1] [c_1\xi + c_2\xi^2 + \mathcal{O}(\xi^3)] \\ &= \sum_{n \geq 1} c_n \epsilon^{n+1} \int_0^1 dt [\chi(t) - 1] t^n \\ &= c_1 \epsilon^2 \int_0^1 dt [\chi(t) - 1] t + c_2 \epsilon^3 \int_0^1 dt [\chi(t) - 1] t^2 + \mathcal{O}(\epsilon^4). \end{aligned} \quad (\text{A31})$$

Therefore, if χ is chosen such that $\int_0^1 dt [\chi(t) - 1] t = 0$, the quadratic term $\sim \epsilon^2$ vanishes and the leading bias becomes cubic. A simple quartic example is

$$\chi(t) = 12t^2 - 20t^3 + 9t^4, \quad 0 \leq t \leq 1, \quad (\text{A32})$$

which satisfies $\chi(0) = 0$, $\chi'(0) = 0$, $\chi(1) = 1$, $\chi'(1) = 0$, and $\int_0^1 dt [\chi(t) - 1] t = 0$. Its bias then scales as

$$\boxed{\text{Bias}(\widehat{O}_\epsilon) = \mathcal{O}(\epsilon^3)}. \quad (\text{A33})$$

Because $\chi_\epsilon(\xi)$ still vanishes at the node and equals 1 outside the ϵ -neighborhood, the inner region contributes only a finite constant to the second moment, while the outer region retains the same logarithmic behavior as before, so

$$\boxed{\text{Var}(\widehat{O}_\epsilon) \sim \log\left(\frac{\xi_0}{\epsilon}\right)}. \quad (\text{A34})$$

6. Polynomial ansatz and higher-order bias cancellation

While the smooth cutoff need not be polynomial (it could be a spline, a trigonometric function or another smooth function), a polynomial ansatz is convenient because all constraints reduce to linear equations for its coefficients so that the bias-cancellation conditions can be imposed analytically. Let

$$\chi(t) = \sum_{j=0}^d a_j t^j, \quad 0 \leq t \leq 1. \quad (\text{A35})$$

If we want the bias to start at order ϵ^{m+2} ($m = 1, 2, \dots$), then the first m moments must vanish:

$$M_n[\chi] \equiv \int_0^1 dt [\chi(t) - 1] t^n = 0, \quad n = 1, \dots, m. \quad (\text{A36})$$

Together with endpoint conditions such as

$$\chi(0) = 0, \quad \chi'(0) = 0, \quad \chi(1) = 1, \quad \chi'(1) = 0, \quad (\text{A37})$$

these constraints define a linear system for the coefficients $\{a_j\}$. The endpoint conditions give, for example,

$$a_0 = 0, \quad a_1 = 0, \quad \sum_{j=0}^d a_j = 1, \quad \sum_{j=1}^d j a_j = 0. \quad (\text{A38})$$

Likewise, substituting the polynomial ansatz Eq. (A35) into the moment condition Eq. (A36) yields

$$\int_0^1 dt \chi(t) t^n = \sum_{j=0}^d a_j \int_0^1 dt t^{n+j} = \sum_{j=0}^d \frac{a_j}{n+j+1}. \quad (\text{A39})$$

Since

$$M_n[\chi] = 0 \iff \int_0^1 dt \chi(t) t^n = \int_0^1 t^n dt = \frac{1}{n+1}, \quad (\text{A40})$$

each moment constraint becomes the linear equation

$$\sum_{j=0}^d \frac{a_j}{j+n+1} = \frac{1}{n+1}, \quad n = 1, \dots, m. \quad (\text{A41})$$

Collecting all endpoint and moment conditions gives a matrix equation

$$\mathbf{A}\mathbf{a} = \mathbf{b}, \quad (\text{A42})$$

with $\mathbf{a} = (a_0, \dots, a_d)^T$ and \mathbf{b} the vector encoding the constraints. If d is larger than strictly necessary, that is, $d+1 > N_c$, where $N_c = m+4$ is the total number of constraints, the system is underdetermined and one obtains a family of admissible smooth cutoffs. For the example given in Eq. (A32), the matrix A is square and has a unique solution since a degree-4 polynomial has 5 coefficients and we imposed 5 constraints. In practice, canceling only the leading moment is often already sufficient and provides a good compromise between bias reduction and numerical robustness (as the smooth cutoff becomes increasingly oscillatory (in the interval $0 \leq t < 1$) as more moments are canceled).

7. Summary of asymptotic scalings

For the near-node behavior $O \sim \xi^{-2}$, the estimators discussed above have the following asymptotic scalings:

estimator	variance	bias
$O(\mathbf{r})$	ξ_c^{-1}	0
\tilde{O}	$\log(\xi_0/\xi_c)$	0
$\tilde{O}_\epsilon^{(1)}, \tilde{O}_\epsilon^{(2)}$	$\log(\xi_0/\epsilon)$	$\mathcal{O}(\epsilon^2)$
$\hat{O}_\epsilon = \chi_\epsilon \tilde{O}$	$\log(\xi_0/\epsilon)$	$\mathcal{O}(\epsilon^{m+2})$

(A43)

where ξ_c is a formal short-distance cutoff used only to display the divergence of unregularized estimators, and m denotes the number of canceled bias moments of the smooth cutoff χ .

8. Practical choice of the regularization parameter ϵ

In practice, the cutoff parameter ϵ plays the role of a bias-variance trade-off parameter. As shown above, the smooth-cutoff regularized estimators satisfy

$$\text{Var}(\hat{O}_\epsilon) \sim \log(\xi_0/\epsilon), \quad \text{Bias}(\hat{O}_\epsilon) \sim \epsilon^{m+2}, \quad (\text{A44})$$

where, again, m is the number of canceled bias moments of the cutoff function. The mean-squared error (MSE) therefore behaves as

$$\text{MSE}(\epsilon) = \underbrace{\text{Var}(\hat{O}_\epsilon)/N}_{\text{statistical error}^2} + \underbrace{\text{Bias}(\hat{O}_\epsilon)^2}_{\text{systematic error}^2} \sim \log(\xi_0/\epsilon)/N + \epsilon^{2(m+2)}, \quad (\text{A45})$$

which shows that decreasing ϵ reduces the bias but increases the variance.

In the limit of $\epsilon \rightarrow 0$, the estimator approaches the unregularized one and the variance reduction disappears. Conversely, choosing ϵ too large suppresses the outliers but introduces a sizeable systematic bias. A practical value of ϵ must therefore lie in an intermediate regime where the regularization is “active” but the bias remains negligible compared to the statistical uncertainty. In practice, ϵ can be chosen by evaluating the estimator for a small set of (decreasing) ϵ values. The optimal region is identified when the mean stabilizes, while the variance remains reduced compared to the unregularized estimator. One then selects ϵ as the largest value for which the bias is below the statistical error, while still providing some variance reduction and thus a non-zero fraction of regularized samples.

Appendix B: Gradient-to-Laplacian identity

We derive the gradient-to-Laplacian identity given in Eq. (33), that we rewrite here for completeness,

$$2\partial_{x_\alpha} v(x) = \nabla_{\mathbf{x}}^2 [x_\alpha v(x)] - \frac{x_\alpha}{x} f''(x), \quad f(x) \equiv xv(x), \quad (\text{B1})$$

valid for $x \neq 0$ in \mathbb{R}^3 , with $x = |\mathbf{x}|$ and for some function $v(x)$. Using $\partial_{x_\beta} x_\alpha = \delta_{\alpha\beta}$ and Einstein summation notation, we get

$$\begin{aligned}\nabla_{\mathbf{x}}^2 [x_\alpha v(x)] &= \partial_{x_\beta} \partial_{x_\beta} [x_\alpha v(x)] \\ &= \partial_{x_\beta} (\delta_{\alpha\beta} v(x) + x_\alpha \partial_{x_\beta} v(x)) \\ &= \partial_{x_\alpha} v(x) + \partial_{x_\beta} [x_\alpha \partial_{x_\beta} v(x)] \\ &= \partial_{x_\alpha} v(x) + \delta_{\alpha\beta} \partial_{x_\beta} v(x) + x_\alpha \partial_{x_\beta} \partial_{x_\beta} v(x) \\ &= 2\partial_{x_\alpha} v(x) + x_\alpha \nabla_{\mathbf{x}}^2 v(x).\end{aligned}\tag{B2}$$

The radial Laplacian (in three-dimension) is derived as follows

$$\nabla_{\mathbf{x}} v(x) = v'(x) \nabla_{\mathbf{x}} x = v'(x) \frac{\mathbf{x}}{x},\tag{B3}$$

$$\nabla_{\mathbf{x}}^2 v(x) = \nabla_{\mathbf{x}} \cdot \left(v'(x) \frac{\mathbf{x}}{x} \right) = \nabla_{\mathbf{x}} v'(x) \cdot \frac{\mathbf{x}}{x} + v'(x) \nabla_{\mathbf{x}} \cdot \left(\frac{\mathbf{x}}{x} \right) = v''(x) + \frac{2}{x} v'(x),\tag{B4}$$

where we used $\nabla_{\mathbf{x}} v'(x) = v''(x) \mathbf{x}/x$ and $\nabla_{\mathbf{x}} \cdot (\mathbf{x}/x) = (\nabla_{\mathbf{x}} \cdot \mathbf{x})/x + \mathbf{x} \cdot \nabla_{\mathbf{x}} (1/x) = 3/x - 1/x = 2/x$ (since $\nabla_{\mathbf{x}} (1/x) = -\mathbf{x}/x^3$). Now introduce $f(x) = xv(x)$. A direct differentiation gives

$$f''(x) = \frac{d^2}{dx^2} [xv(x)] = \frac{d}{dx} [v(x) + xv'(x)] = 2v'(x) + xv''(x),\tag{B5}$$

so Eq. (B4) can be written as

$$\nabla_{\mathbf{x}}^2 v(x) = \frac{1}{x} f''(x).\tag{B6}$$

Substituting Eq. (B6) into Eq. (B2) yields

$$\nabla_{\mathbf{x}}^2 [x_\alpha v(x)] = 2\partial_{x_\alpha} v(x) + \frac{x_\alpha}{x} f''(x),\tag{B7}$$

which rearranges to Eq. (B1).

Appendix C: Divergence theorem identities

We adopt in this appendix a more math-based notation, in particular without putting vectors in bold font. Let $x \in \Omega$ denote a configuration-space sample (e.g. $x \equiv \mathbf{r} \in \mathbb{R}^{3N}$ in VMC), with domain $\Omega = \mathbb{R}^d$ for open boundary conditions, or a periodic simulation cell under periodic boundary conditions. Let $\pi(x) \geq 0$ be an unnormalized probability distribution on Ω , with normalization $Z = \int_{\Omega} \pi(x) dx$. For an observable O , we write $\langle O \rangle \equiv \langle O \rangle_{\pi} = Z^{-1} \int_{\Omega} O(x) \pi(x) dx$. For a sufficiently regular vector field $A : \Omega \rightarrow \mathbb{R}^d$, define the Langevin Stein operator⁵⁹

$$\mathcal{L}_{\pi}[A](x) \equiv \nabla \cdot A(x) + A(x) \cdot \nabla \log \pi(x),\tag{C1}$$

where $\nabla \equiv \nabla_x$ is the configuration-space gradient. Throughout this section, we assume boundary conditions such that the divergence theorem can be applied to the vector field entering each identity without producing residual boundary terms. Concretely, for open boundary conditions, it means that the relevant field $\pi(x)A(x)H(x)$, defined below for some indicator function H , decays sufficiently rapidly as $|x| \rightarrow \infty$, while for periodic boundary conditions, $\pi(x)$, $A(x)$ and $H(x)$ are periodic on Ω . In each subsection below, we present an identity with an associated (boxed) example.

1. Codimension-0: zero-mean control variate

Consider the vector field

$$F(x) = \pi(x)A(x).\tag{C2}$$

By the divergence theorem and the above boundary assumptions,

$$\int_{\Omega} \nabla \cdot F(x) dx = \int_{\partial\Omega} F \cdot ndS = 0.\tag{C3}$$

Using $\nabla \cdot (\pi A) = \pi(\nabla \cdot A + A \cdot \nabla \log \pi) = \pi \mathcal{L}_\pi[A]$, we obtain $\langle \mathcal{L}_\pi[A] \rangle = 0$, so for any observable O ,

$$\langle O \rangle = \langle O + \mathcal{L}_\pi[A] \rangle. \quad (\text{C4})$$

Thus $\mathcal{L}_\pi[A]$ is a zero-mean control variate correction, which can reduce the estimator variance when the vector field A is chosen appropriately.

Box 1: Example: forces under open boundary conditions

Consider $x \equiv \mathbf{r} = (\mathbf{r}_1, \dots, \mathbf{r}_N)$, $\pi(\mathbf{r}) = |\Psi(\mathbf{r})|^2$, and a nucleus I of charge Z_I at a fixed position \mathbf{R}_I . We denote the gradient and Laplacian respectively as $\nabla \equiv \nabla_{\mathbf{r}}$ and $\nabla^2 \equiv \sum_{i\alpha} \partial^2 / \partial r_{i\alpha}^2$. The bare electron-nucleus Hellmann-Feynman force on nucleus I along the direction α is

$$F_{I\alpha, en}^{\text{HF}}(\mathbf{r}) = Z_I \sum_i \frac{r_{i\alpha} - R_{I\alpha}}{|\mathbf{r}_i - \mathbf{R}_I|^3}, \quad (\text{C5})$$

which is singular as $|\mathbf{r}_i - \mathbf{R}_I| \rightarrow 0$. The choice of \mathbf{A} made in the work of Assaraf and Caffarel²⁶ is

$$\mathbf{A}_{I\alpha}(\mathbf{r}) = \nabla Q_{I\alpha}(\mathbf{r}), \quad Q_{I\alpha}(\mathbf{r}) = Z_I \sum_i \frac{r_{i\alpha} - R_{I\alpha}}{|\mathbf{r}_i - \mathbf{R}_I|}. \quad (\text{C6})$$

Note that with a reasonable wave function choice, $\pi(\mathbf{r})\mathbf{A}_{I\alpha}(\mathbf{r})$ decays sufficiently fast at infinity so that the boundary term vanishes, thus satisfying the boundary assumption. Using the identity $\nabla^2((r_{i\alpha} - R_{I\alpha})/|\mathbf{r}_i - \mathbf{R}_I|) = -2(r_{i\alpha} - R_{I\alpha})/|\mathbf{r}_i - \mathbf{R}_I|^3$ (for $\mathbf{r}_i \neq \mathbf{R}_I$), one then finds that $\nabla \cdot \mathbf{A}_{I\alpha} = \nabla^2 Q_{I\alpha} = -2F_{I\alpha, en}^{\text{HF}}$, meaning that this divergence part of $\mathcal{L}_\pi[\mathbf{A}_{I\alpha}]$ cancels the Coulomb singular term in Eq. (C5) exactly (provided it is rescaled by a factor of 2, which is possible because by construction $\langle \mathcal{L}_\pi[\mathbf{A}_{I\alpha}] \rangle = 0$ implies that $\langle \mathcal{L}_\pi[\mathbf{A}_{I\alpha}]/2 \rangle = 0$). Inserting into Eq. (C4), the corresponding improved estimator is then

$$F_{I\alpha}^{\text{imp}}(\mathbf{r}) = F_{I\alpha}^{\text{HF}}(\mathbf{r}) + \mathcal{L}_\pi[\mathbf{A}_{I\alpha}](\mathbf{r})/2 = F_{I\alpha, nn}^{\text{HF}}(\mathbf{R}) + \nabla Q_{I\alpha}(\mathbf{r}) \cdot \nabla \log |\Psi(\mathbf{r})|, \quad (\text{C7})$$

which is unbiased because $\langle \mathcal{L}_\pi[\mathbf{A}] \rangle = 0$, and it has much smaller variance because the singular term $F_{I\alpha, en}^{\text{HF}}(\mathbf{r})$, given in Eq. (C5), is exactly canceled, and only the constant nucleus-nucleus term $F_{I\alpha, nn}^{\text{HF}}(\mathbf{R})$ survives from the bare estimator $F_{I\alpha}^{\text{HF}}(\mathbf{r})$.

2. Codimension-1: surface-to-volume conversion

Let $\xi : \Omega \rightarrow \mathbb{R}$ be differentiable, fix $s \in \mathbb{R}$, and define the Heaviside step function $\theta_s(x) \equiv \theta(s - \xi(x))$, which should be periodized accordingly under periodic boundary conditions. Consider the truncated vector field

$$F(x) = \pi(x)\theta_s(x)A(x). \quad (\text{C8})$$

Applying the divergence theorem on Ω gives, as before, $\int_\Omega \nabla \cdot F dx = 0$. Expanding $\nabla \cdot F = \nabla \cdot (\pi\theta_s A)$ via the product rule yields

$$\nabla \cdot (\pi\theta_s A) = \pi\theta_s \mathcal{L}_\pi[A] + \pi(\nabla\theta_s) \cdot A. \quad (\text{C9})$$

Using $\nabla\theta_s = \nabla_x \theta(s - \xi(x)) = -\delta(s - \xi)\nabla\xi$ (since $\partial_t \theta(t) = \delta(t)$), we obtain the identity

$$\langle \delta(s - \xi)A \cdot \nabla\xi \rangle = \langle \theta_s \mathcal{L}_\pi[A] \rangle. \quad (\text{C10})$$

For observables involving a single delta function of the form $\langle \delta(s - \xi(x))W(x) \rangle$ (e.g. (multipole) densities, pair correlations, angular distributions), one typically chooses A such that on $\{\xi = s\}$, $A(x; s) \cdot \nabla\xi(x) = W(x)$. A simple choice is

$$A(x; s) = W(x) \frac{\nabla\xi(x)}{|\nabla\xi(x)|^2}, \quad (\text{C11})$$

provided $\nabla\xi \neq 0$. With this choice, the left-hand side of Eq. (C10) reduces to $\langle \delta(s - \xi)W \rangle$, while the right-hand side is a sublevel-set (volume) average over $\{\xi \leq s\}$. We emphasize that Eq. (C10) turns an integration over a shell into an integration over a ball, therefore increasing the signal-to-noise ratio in numerical calculations.

Box 2: Example: pair correlation functions

For a system of particles with positions $\{\mathbf{r}_i\}$, the bare radial pair correlation function estimator is $g(s) \propto \sum_{i < j} \delta(s - r_{ij})$, $r_{ij} = |\mathbf{r}_i - \mathbf{r}_j|$. To apply Eq. (C10), fix a pair (i, j) and set $\xi(x) = r_{ij}(x)$. The configuration space gradient is

$$\nabla r_{ij} = (0, \dots, \underbrace{\hat{\mathbf{r}}_{ij}}_{\mathbf{r}_i \text{ block}}, \dots, \underbrace{-\hat{\mathbf{r}}_{ij}}_{\mathbf{r}_j \text{ block}}, \dots, 0), \quad \hat{\mathbf{r}}_{ij} = \frac{\mathbf{r}_i - \mathbf{r}_j}{r_{ij}}, \quad (\text{C12})$$

so that $|\nabla r_{ij}|^2 = |\hat{\mathbf{r}}_{ij}|^2 + |-\hat{\mathbf{r}}_{ij}|^2 = 2$. A convenient choice of the vector field satisfying $\mathbf{A}_{ij} \cdot \nabla r_{ij} = 1$ on $\{r_{ij} = s\}$ is therefore

$$\mathbf{A}_{ij}(x) = \frac{\nabla r_{ij}}{|\nabla r_{ij}|^2} = \frac{1}{2}(0, \dots, \hat{\mathbf{r}}_{ij}, \dots, -\hat{\mathbf{r}}_{ij}, \dots, 0). \quad (\text{C13})$$

Note that, to further regularize short-distances, one can in principle scale A_{ij} by a smooth shaping factor $g(r_{ij}; s)$, provided $g(s; s) = 1$. We now evaluate $\mathcal{L}_\pi[\mathbf{A}_{ij}] = \nabla \cdot \mathbf{A}_{ij} + \mathbf{A}_{ij} \cdot \nabla \log \pi$. Using $\nabla_{\mathbf{r}_i} \cdot \hat{\mathbf{r}}_{ij} = 2/r_{ij}$ and $\nabla_{\mathbf{r}_j} \cdot \hat{\mathbf{r}}_{ij} = -2/r_{ij}$ we obtain $\nabla \cdot \mathbf{A}_{ij} = 2/r_{ij}$. The second term becomes a relative drift term, so inserting these expressions into Eq. (C10) gives, for a single pair (i, j) ,

$$\langle \delta(s - r_{ij}) \rangle = \left\langle \theta(s - r_{ij}) \left(\frac{2}{r_{ij}} + \hat{\mathbf{r}}_{ij} \cdot (\nabla_i - \nabla_j) \log \Psi \right) \right\rangle \quad (\text{VMC, } \pi = |\Psi|^2). \quad (\text{C14})$$

For classical NVT sampling methods, such as classical Monte Carlo (MC) or molecular dynamics (MD), with $\pi \propto e^{-\beta U}$ and $\nabla_i \log \pi = \beta \mathbf{F}_i^{\text{cl}}$, the improved estimator is

$$\langle \delta(s - r_{ij}) \rangle = \left\langle \theta(s - r_{ij}) \left(\frac{2}{r_{ij}} + \frac{\beta}{2} \hat{\mathbf{r}}_{ij} \cdot (\mathbf{F}_i^{\text{cl}} - \mathbf{F}_j^{\text{cl}}) \right) \right\rangle \quad (\text{MD/MC, } \pi = e^{-\beta U}). \quad (\text{C15})$$

Summing over all pairs $(i < j)$ and applying the proper normalization yields the corresponding improved estimator for $g(s)$.

3. Codimension-2: intersection-to-volume conversion

We now consider observables involving two delta constraints of the generic form

$$g(s, t) = \langle \delta(s - \xi(x)) \delta(t - \eta(x)) \rangle, \quad (\text{C16})$$

for differentiable function $\xi, \eta : \Omega \rightarrow \mathbb{R}$ and constants $s, t \in \mathbb{R}$. These estimators are supported on the intersection $\{\xi = s\} \cap \{\eta = t\}$. Define

$$\theta_s(x) \equiv \theta(s - \xi(x)), \quad \theta_t(x) \equiv \theta(t - \eta(x)), \quad \delta_s(x) \equiv \delta(s - \xi(x)), \quad \delta_t(x) \equiv \delta(t - \eta(x)), \quad (\text{C17})$$

and let $p = \nabla\xi$, $q = \nabla\eta$, so that $\nabla\theta_s = -\delta_s p$ and $\nabla\theta_t = -\delta_t q$.

First elimination. Applying the divergence theorem to the doubly truncated vector field

$$F_A(x) = \pi(x) \theta_s(x) \theta_t(x) A(x), \quad (\text{C18})$$

yields $\int_\Omega \nabla \cdot F_A dx = 0$, given our initial boundary assumptions. Expanding gives

$$\nabla \cdot (\pi \theta_s \theta_t A) = \pi \theta_s \theta_t \mathcal{L}_\pi[A] - \pi \delta_s \theta_t (A \cdot p) - \pi \theta_s \delta_t (A \cdot q). \quad (\text{C19})$$

To eliminate one surface term, without loss of generality, we choose A such that (we will come back to this choice later, causing asymmetry in the final expression)

$$A \cdot p = 1 \quad \text{and} \quad A \cdot q = 0. \quad (\text{C20})$$

In that case, integrating over Ω and dividing by the normalization Z , we get

$$\langle \delta_s \theta_t \rangle = \langle \theta_s \theta_t \mathcal{L}_\pi[A] \rangle. \quad (\text{C21})$$

We now differentiate this expression with respect to t , noting that A and $\mathcal{L}_\pi[A]$ are independent of t , to reach the intermediate expression

$$\langle \delta_s \delta_t \rangle = \langle \theta_s \delta_t \mathcal{L}_\pi[A] \rangle. \quad (\text{C22})$$

Second elimination. As we are still left with one delta function on the right-hand side of Eq. (C22), we proceed to eliminate it by applying a second time the divergence theorem, but this time to the new vector field (defined in such a way to be able to use the intermediate identity Eq. (C22))

$$F_B(x) = \pi(x) \theta_s(x) \theta_t(x) B(x) \mathcal{L}_\pi[A](x). \quad (\text{C23})$$

Applying the divergence theorem to F_B gives $\int_\Omega \nabla \cdot F_B dx = 0$. Expanding again using the product rule, we get two volume and two surface terms

$$\nabla \cdot (\pi \theta_s \theta_t B \mathcal{L}_\pi[A]) = \pi \theta_s \theta_t \left\{ \mathcal{L}_\pi[B] \mathcal{L}_\pi[A] + B \cdot \nabla \mathcal{L}_\pi[A] \right\} - \pi \left\{ \delta_s \theta_t (B \cdot p) + \theta_s \delta_t (B \cdot q) \right\} \mathcal{L}_\pi[A]. \quad (\text{C24})$$

To be able to use the identity given in Eq. (C22), we choose B such that

$$B \cdot p = 0 \quad \text{and} \quad B \cdot q = 1. \quad (\text{C25})$$

Applying these constraints, integrating over Ω and dividing by Z , we get

$$\langle \theta_s \delta_t \mathcal{L}_\pi[A] \rangle = \langle \theta_s \theta_t (\mathcal{L}_\pi[B] \mathcal{L}_\pi[A] + B \cdot \nabla \mathcal{L}_\pi[A]) \rangle. \quad (\text{C26})$$

We can finally combine Eqs. (C22) and (C26) to obtain an expression that is now free of delta functions, that is,

$$\langle \delta_s \delta_t \rangle = \langle \theta_s \theta_t (\mathcal{L}_\pi[B] \mathcal{L}_\pi[A] + B \cdot \nabla \mathcal{L}_\pi[A]) \rangle. \quad (\text{C27})$$

Given that we eliminated the two delta functions sequentially, the expression is manifestly asymmetric, as previously alluded to. This can be mathematically seen even better by writing the expression in parentheses as $\mathcal{L}_\pi[B] \mathcal{L}_\pi[A] + B \cdot \nabla \mathcal{L}_\pi[A] = \mathcal{L}_\pi[B \mathcal{L}_\pi[A]]$, the latter clearly identifying that B was introduced after weighting by $\mathcal{L}_\pi[A]$. If instead δ_t is first removed with B and then δ_s is removed with A , the two theta functions would be multiplied by $\mathcal{L}_\pi[A \mathcal{L}_\pi[B]]$ instead of $\mathcal{L}_\pi[B \mathcal{L}_\pi[A]]$. We can therefore average the two orderings to obtain the symmetric formula

$$\boxed{\langle \delta_s \delta_t \rangle = \left\langle \theta_s \theta_t \frac{1}{2} (\mathcal{L}_\pi[A \mathcal{L}_\pi[B]] + \mathcal{L}_\pi[B \mathcal{L}_\pi[A]]) \right\rangle}, \quad (\text{C28})$$

which is now indeed manifestly symmetric under swapping $(A, \xi, s) \leftrightarrow (B, \eta, t)$. In addition, one can use the identity $\mathcal{L}_\pi[\phi A] = \mathcal{L}_\pi[A] \phi + A \cdot \nabla \phi$, for some scalar ϕ , to expand this expression (and facilitate computer implementation).

Constructing the vector fields A and B . We started with the level-set constraints $\xi(x) = s$ and $\eta(x) = t$, and denoted their gradients by $p = \nabla \xi$ and $q = \nabla \eta$, which (when linearly independent) span the 2D normal subspace associated with the two constraints in configuration space. The only requirements that define A and B , given in Eqs. (C20) and (C25), are dot products with p and q . It is therefore a natural choice to take A and B to be inside $\text{span}(\{p, q\})$ (in particular, neglecting tangent components to both constraints), meaning that

$$A = ap + bq \quad \text{and} \quad B = cp + dq, \quad (\text{C29})$$

for $a, b, c, d \in \mathbb{R}$. Substituting first this form of A into the dot product constraints given in Eq. (C20) gives the following two equations

$$(ap + bq) \cdot p = a(p \cdot p) + b(q \cdot p) = 1, \quad (\text{C30})$$

$$(ap + bq) \cdot q = a(p \cdot q) + b(q \cdot q) = 0, \quad (\text{C31})$$

$$(\text{C32})$$

which in matrix form reads

$$G \begin{pmatrix} a \\ b \end{pmatrix} = \begin{pmatrix} 1 \\ 0 \end{pmatrix}, \quad G = \begin{pmatrix} p \cdot p & q \cdot p \\ p \cdot q & q \cdot q \end{pmatrix}, \quad (\text{C33})$$

where G is the Gram matrix. Solving for the coefficients

$$\begin{pmatrix} a \\ b \end{pmatrix} = G^{-1} \begin{pmatrix} 1 \\ 0 \end{pmatrix}, \quad G^{-1} = \frac{1}{|G|} \begin{pmatrix} q \cdot q & -q \cdot p \\ -p \cdot q & p \cdot p \end{pmatrix}, \quad (\text{C34})$$

where $|G| = \det(G) = (p \cdot p)(q \cdot q) - (p \cdot q)^2$, we obtain

$$A = \frac{(q \cdot q)p - (p \cdot q)q}{|G|}. \quad (\text{C35})$$

Proceeding similarly for B , using Eq. (C25), we obtain

$$B = \frac{-(q \cdot p)p + (p \cdot p)q}{|G|}. \quad (\text{C36})$$

Selecting A to satisfy $A \cdot p = 1$ and $A \cdot q = 0$ makes A have unit flux through the ξ -level set while remaining tangent to the η -level set, while selecting B with $B \cdot p = 0$ and $B \cdot q = 1$ enforces the complementary property. This is essential because a single application of the divergence theorem produces codimension-1 boundary terms, while the dual constraints imposed isolate the desired boundary (intersection) contribution.

Higher codimension. The procedure obviously generalizes to observables with k -delta functions, of the form

$$g(\mathbf{s}) = \left\langle \prod_{a=1}^k \delta(s_a - \xi_a(x)) \right\rangle, \quad (\text{C37})$$

where the gradients $p_a = \nabla \xi_a \in \mathbb{R}^d$ can be defined. However, eliminating delta functions sequentially increases the highest derivative order in the estimator linearly with k , which quickly becomes impractical as k grows. A compromise would be to eliminate one (or a few) delta functions analytically and treat the remaining variables with the usual binning or kernel smoothing approaches.

Box 3: Example: angular distribution functions

A common structural observable is an angular distribution function (and its variants) built from particle triplet indices (i, j, k) . One convenient codimension-2 example is the joint distribution of a bond length and an angle,

$$C(s, t) \propto \left\langle \sum_{(i,j,k)} \delta(s - r_{ij}) \delta(t - c_{ijk}) \right\rangle, \quad c_{ijk} \equiv \cos \theta_{ijk} = \frac{\mathbf{r}_{ij} \cdot \mathbf{r}_{ik}}{r_{ij} r_{ik}}. \quad (\text{C38})$$

Here $\xi = r_{ij}$ and $\eta = c_{ijk}$, so (C28) converts the intersection estimator supported on $\{r_{ij} = s\} \cap \{c_{ijk} = t\}$ into a volume average over $\{r_{ij} \leq s, c_{ijk} \leq t\}$ plus drift/divergence terms, yielding an unbiased variance-reduced alternative to direct binning. It is possible to derive the associated A and B vector fields using Eqs. (C35) and (C36) respectively.

Appendix D: Periodic alternative for the Q-function

In this section, we present the estimator proposed by Qian *et al.*²³ that we compared with in Fig. 3. Instead of providing an explicit expression for the \mathbf{Q} -function (as defined in Eq. (42) in our case), the authors implicitly define \mathbf{Q} by providing an expression for its gradient. The expression reads as follows

$$\partial_{i\alpha} Q_{I\beta} = - \sum_{\mathbf{T}} Z_I \left[\frac{\operatorname{erfc}(\kappa r_{i\mathbf{T}})}{r_{i\mathbf{T}}^3} r_{i\mathbf{T},\beta} r_{i\mathbf{T},\alpha} - \delta_{\alpha\beta} \frac{\operatorname{erfc}(\kappa r_{i\mathbf{T}})}{r_{i\mathbf{T}}} - \delta_{\alpha\beta} \frac{\kappa}{\sqrt{\pi}} \operatorname{Ei}(-\kappa^2 r_{i\mathbf{T}}^2) \right], \quad (\text{D1})$$

where $r_{i\mathbf{T}} \equiv |\mathbf{r}_i - \mathbf{R}_I - \mathbf{T}|$, $\partial_{i\alpha} \equiv \partial/\partial r_{i\alpha}$, and $\alpha, \beta \in \{x, y, z\}$. In vector form, the gradient of the x -component, for example, can be written explicitly as

$$\nabla_i Q_{Ix} = - \sum_{\mathbf{T}} Z_I \begin{pmatrix} \frac{\operatorname{erfc}(\kappa r_{i\mathbf{T}}) r_{i\mathbf{T},x}^2}{r_{i\mathbf{T}}^3} - \frac{\operatorname{erfc}(\kappa r_{i\mathbf{T}})}{r_{i\mathbf{T}}} - \frac{\kappa}{\sqrt{\pi}} \operatorname{Ei}(-\kappa^2 r_{i\mathbf{T}}^2) \\ \frac{\operatorname{erfc}(\kappa r_{i\mathbf{T}}) r_{i\mathbf{T},x} r_{i\mathbf{T},y}}{r_{i\mathbf{T}}^3} \\ \frac{\operatorname{erfc}(\kappa r_{i\mathbf{T}}) r_{i\mathbf{T},x} r_{i\mathbf{T},z}}{r_{i\mathbf{T}}^3} \end{pmatrix}. \quad (\text{D2})$$

The Laplacian of $Q_{I\beta}$ with respect to r_i is obtained by taking the divergence of the above expression, i.e. $\nabla_i^2 Q_{I\beta} = \nabla_i \cdot \nabla_i Q_{I\beta}$. Carrying out the differentiation analytically, one finds the closed-form expression

$$\nabla_i^2 Q_{I\beta} = -2 \sum_{\mathbf{T}} Z_I r_{i\mathbf{T},\beta} \left[\frac{\operatorname{erfc}(\kappa r_{i\mathbf{T}})}{r_{i\mathbf{T}}^3} - \frac{\kappa}{\sqrt{\pi}} \frac{\exp(-\kappa^2 r_{i\mathbf{T}}^2)}{r_{i\mathbf{T}}^2} \right]. \quad (\text{D3})$$

While not directly provided in the aforementioned paper, the associated \mathbf{Q} -function components are given by

$$Q_{I\beta}(\mathbf{r}) = Z_I \sum_i \sum_{\mathbf{T}} r_{i\mathbf{T},\beta} \left(\frac{\operatorname{erfc}(\kappa r_{i\mathbf{T}})}{r_{i\mathbf{T}}} + \frac{\kappa}{\sqrt{\pi}} \operatorname{Ei}(-\kappa^2 r_{i\mathbf{T}}^2) \right), \quad (\text{D4})$$

where the exponential integral (Ei) term is an extra contribution that is absent in our definition of the \mathbf{Q} -function in Eq. (42).